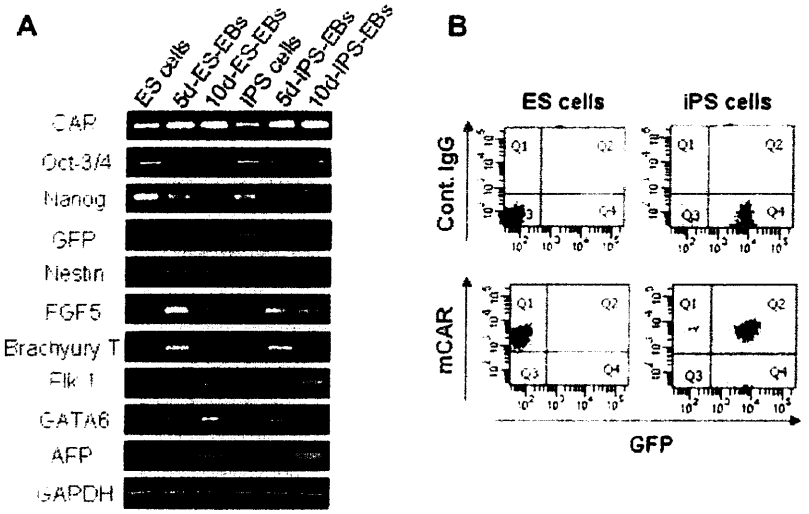

Figure 1. Gene expression patterns of mouse iPS cells were similar to those of mouse ES cells. (A): Total RNA was isolated from mouse ES cells (lane 1), 5d-ES-EBs (lane 2), 10d-ES-EBs (lane 3), iPS cells (lane 4), 5d-iPS-EBs (lane 5), or 10d-iPS-EBs (lane 6), and semiquantitative reverse transcriptase-polymerase chain reaction was then performed as described in Materials and Methods. The primers for Oct-3/4 and Nanog amplified both endogenous gene and exogenous factors. (B): The expression levels of CAR in mouse ES cells and iPS cells were detected with anti-mouse CAR monoclonal antibody by flow cytometry. As a negative control, the cells were incubated with an irrelevant antibody. Data shown are from one representative experiment of three performed. Abbreviations: AFP, α-fetoprotein; CAR, coxsackievirus and adenovirus receptor; Cont., control; EB, embryoid body; ES, embryonic stem; 5d-ES-EBs, ES cell-derived 5-day-cultured EBs; 10d-ES-EBs, ES cell-derived 10-day-cultured EBs; FGF, fibroblast growth factor; GAPDH, glyceraldehyde-3-phosphate dehydrogenase; GATA, GATA-binding protein; GFP, green fluorescent protein; iPS, induced pluripotent stem; 5d-iPS-EBs, iPS cell-derived 5-day-cultured EBs; 10d-iPS-EBs, iPS cell-derived 10-day-cultured EBs; mCAR, mouse CAR.

LacZ-transduced ES cells successfully expressed LacZ (Fig. 2A, top) as described previously [16]. Likewise, the CA and the EF-1α promoter but not the RSV or the CMV promoter exhibited potent transduction activity in iPS cells (Fig. 2A, bottom). Besides mouse iPS cell clone 20D17, mouse iPS cell clones 38C2 and stm99-1, which were generated from MEFs [4] and gastric epithelial cells [26], respectively, also efficiently expressed transgenes by an Ad vector containing the CA or EF-1α promoter (supporting information Fig. S1).

To confirm that the transgene was expressed in GFP-expressing undifferentiated iPS cells, we generated Ad-CA-mCherry and Ad-EF-mCherry, both of which express a monomeric DsRed variant, mCherry. Flow cytometric and fluorescent microscopic analysis showed that the mCherry expression was observed in GFP-expressing iPS cells transduced with Ad-CA-mCherry or Ad-EF-mCherry (Fig. 2B, supporting information Fig. S2). Furthermore, the expression of mCherry in iPS cells was dose-dependent, and more than 90% of the cells expressed mCherry after transduction with 10,000 VPs/cell of Ad-CA-mCherry and Ad-EF-mCherry (Fig. 2C and data not shown). Importantly, there was no significant difference in the percentage of GFP-positive cells between nontransduced cells and Ad-CA-mCherry- or Ad-EF-mCherry-transduced cells (Fig. 2D and data not shown). Moreover, neither alkaline phosphatase activity nor Oct-3/4 expression in iPS cells on day 3 after Ad vector-mediated transduction was different from that in nontransduced cells (supporting information Fig. 3). We also examined the pluripotency of Ad vector-transduced iPS cells by teratoma formation. Mouse iPS cells were transduced with Ad vector and were then injected subcutaneously into the backs of nude mice. After subcutaneous transplantation, we obtained teratomas containing epidermis, cartilage, and gut epithelial tissues (Fig. 2E). These observations demonstrated that the undifferentiated state and pluripotency in iPS cells were still maintained even after Ad vector transduction. Furthermore, we counted the number of viable iPS cells at 24, 48, and 72 hours after transduction to investigate the cytotoxicity in iPS cells transduced with Ad-CA-mCherry at 3,000 or 10,000 VPs/cell. The number of viable iPS cells transduced with Ad-CA-mCherry at 3,000 VPs/cell was comparable to the number of viable nontransduced iPS cells, whereas the number of viable iPS cells was slightly (but not significantly) reduced in Ad-CA-mCherry-transduced iPS cells at 10,000 VPs/cell (Fig. 2F). This result was quite similar to that for ES cells (Fig. 2F), and our data suggest that Ad vector transduction has almost no cytotoxicity against either mouse ES cells or mouse iPS cells. These results clearly demonstrated that an Ad vector containing the CA or the EF-1α promoter is an appropriate vector for both ES cells and iPS cells and that iPS cells have the same features as ES cells in terms of Ad vector-mediated transduction.

Ad Vectors Containing the CA Promoter Robustly Drove Transgene Expression in iPS-EBs

We next performed a transduction experiment for ES-EBs and iPS-EBs using a LacZ-expressing Ad vector. Consistent with our previous report [17], the CA promoter showed the highest LacZ expression in ES-EBs. Similarly, the CA promoter showed the highest transduction efficiency in iPS-EBs (Fig. 3A, 3B). Interestingly, the CMV promoter had strong activity in iPS-EBs despite its weak activity in ES cells, ES-EBs, and undifferentiated iPS cells (Figs. 2A, 3A, 3B). These phenomena were also observed by using other iPS cell clone-derived EBs (supporting information Fig. 4).

We next attempted to express the transgene inside the ES-EBs and iPS-EBs, as it is considered to be essential to express the transgene in the EB interior to differentiate ES cells or iPS cells into functional cells. Thus, ES-EBs and iPS-EBs were transduced in triplicate with Ad-CMV-mCherry or Ad-CA-mCherry. This transduction method, namely the triple transduction method, is a gene transfer method that uses an Ad vector to express the transgene in the EB interior (see

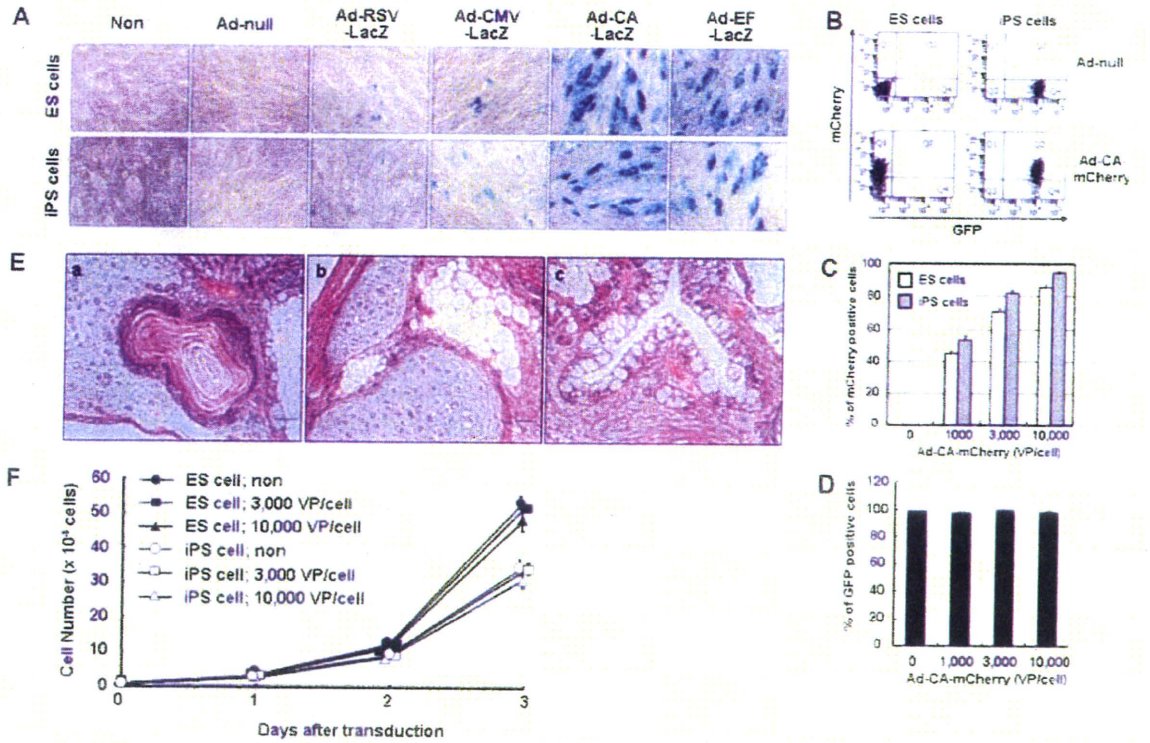

Figure 2. Efficient transgene expression in mouse iPS cells by using an Ad vector containing the CA and the EF-1α promoter. **(A):** Mouse ES cells or iPS cells were transduced with a LacZ-expressing Ad vector at 3,000 VPs/cell. On the following day, X-galactosidase (Gal) staining was carried out. Similar results for X-Gal staining were obtained in three independent experiments. **(B):** Mouse ES cells or iPS cells were transduced with Ad-CA-mCherry at 3,000 VPs/cell, and mCherry-expressing cells were then analyzed by flow cytometry. **(C, D):** Mouse ES cells or iPS cells were transduced with different amounts of Ad-CA-mCherry for 1.5 hours. mCherry expression **(C)** and GFP expression **(D)** were determined by flow cytometry. The data are expressed as the mean ± SD ($n = 3$). **(E):** Paraffin sections of the teratomas derived from Ad-CA-mCherry-transduced iPS cells were prepared, and sections were stained with hematoxylin and eosin: a, ectoderm (epidermis); b, mesoderm (cartilage and adipocyte); c, endoderm (gut epithelium). **(F):** After adenoviral transduction, viable mouse ES cells or iPS cells were counted. Data are expressed as the mean ± SD ($n = 3$). Abbreviations: Ad, adenovirus; CA, cytomegalovirus enhancer/β-actin promoter; CMV, cytomegalovirus; EF elongation factor-1α; ES, embryonic stem; GFP, green fluorescent protein; IPS, induced pluripotent stem; LacZ, β-galactosidase; RSV, Rous sarcoma virus; VP, vector particle.

Materials and Methods) [17]. Confocal microscopic analysis revealed mCherry expression interior in ES-EBs or iPS-EBs by triple transduction, whereas mCherry expression was observed only in the periphery of the ES-EBs or iPS-EBs by single transduction (Fig. 3C). The percentage of mCherry-positive cells in the ES-EBs or iPS-EBs transduced in triplicate with Ad-CA-mCherry was 43% or 56%, respectively, as determined by flow cytometry (Fig. 3C). In addition, confocal microscopic analysis and flow cytometric analysis showed that Ad-CMV-mCherry-transduced ES-EBs expressed little mCherry even using the triple transduction method, whereas iPS-EBs transduced in triplicate with Ad-CMV-mCherry expressed mCherry only in the periphery of the iPS-EBs. These results are in agreement with LacZ expression in Ad-CMV-LacZ-transduced iPS-EBs as described above. Our data demonstrated that, as in the case of ES cells and ES-EBs, the choice of a suitable promoter was important for efficient transduction in iPS cells and iPS-EBs.

Adipocyte and Osteoblast Differentiation of Mouse iPS Cells Was Facilitated by Ad Vector Transduction

We have shown previously that adipocyte differentiation from mouse ES cells is enhanced by the transduction of the *PPARγ* gene, which is known to be a master regulator gene for adipogenesis [18, 19], into ES cells and ES-EBs using an Ad vector. In this study, to examine whether adipocyte differentiation from iPS cells could also be promoted by Ad vector-mediated transduction and to compare the adipogenic potential between ES cells and iPS cells, both types of cells were differentiated into adipocytes by the transduction of the *PPARγ* gene using the triple transduction method described above. Oil red O staining after culturing for 15 days revealed that lipid droplets were accumulated in both ES cell-derived cells and iPS cell-derived cells by culturing with adipogenic supplements, although the level of lipid accumulation in iPS cell-derived cells was lower than that in ES cells-derived cells (Fig. 4A). In the presence of adipogenic supplements, the percentage of oil red O-positive cells in nontransduced or Ad-CA-LacZ-transduced ES-EBs was approximately 50%, whereas 20%-30% of the nontransduced or Ad-CA-LacZ-transduced iPS-EBs were positive for oil red O. Importantly, adipocyte differentiation in Ad-CA-PPARγ-transduced cells was more efficient than that in nontransduced or Ad-CA-LacZ-transduced cells (Fig. 4A). Oil red O-positive cells in Ad-CA-PPARγ-transduced ES cell- or iPS cell-derived cells were more than 90% or 80% of the total cells, respectively. Furthermore, enhanced adipocyte differentiation from PPARγ-transduced ES and iPS cells was also confirmed by measuring the activity of GPDH and the expression of marker genes

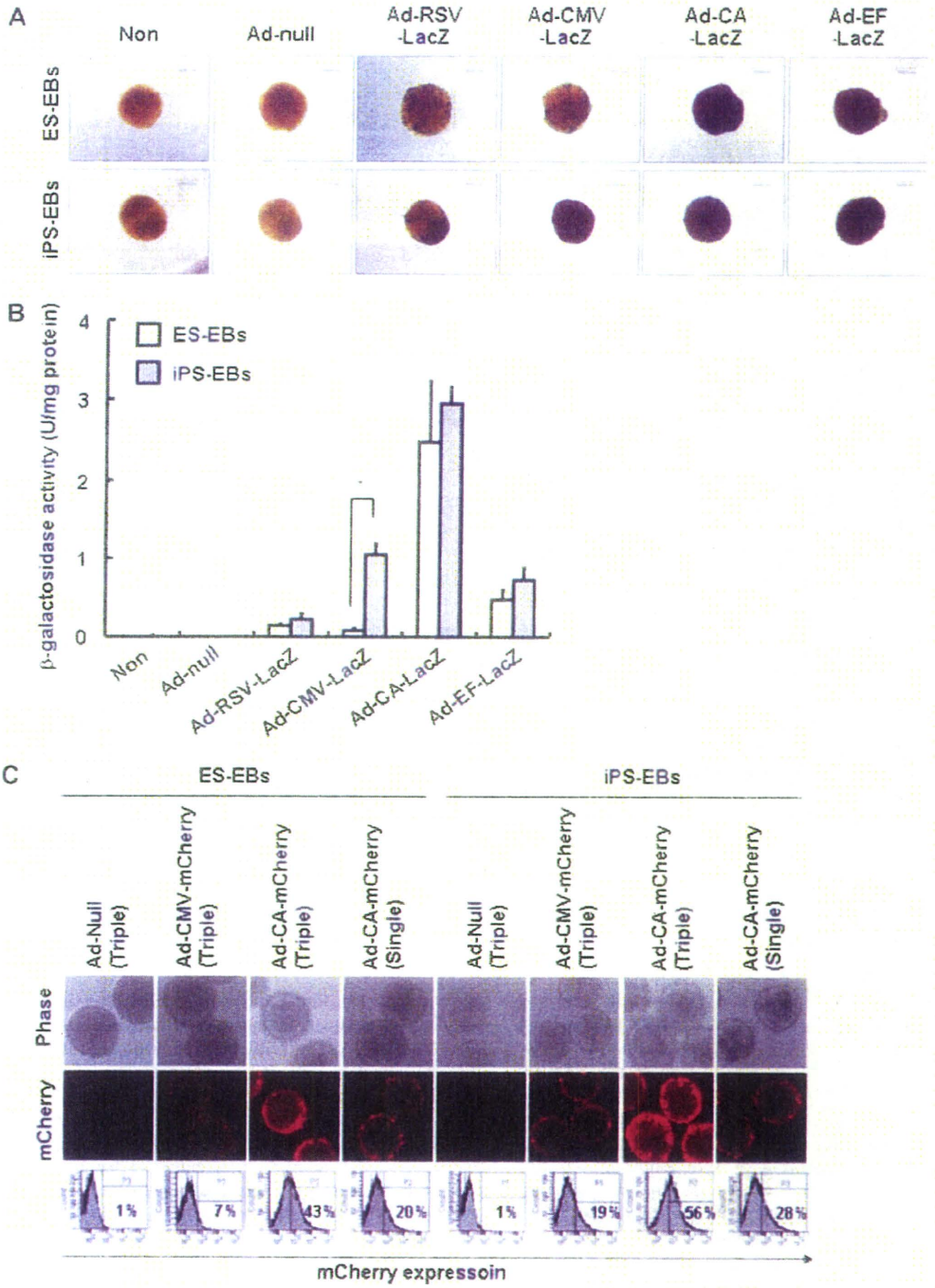

Figure 3. Comparison of promoter activity in iPS-EBs by using Ad vectors. ES cell-derived or IPS cell-derived 5-day-cultured EBs were transduced with each Ad vector at 3,000 vector particles/cell. After 48 hours, X-galactosidase (Gal) staining **(A)** and a *β*-galactosidase luminescence assay **(B)** were performed as described in Materials and Methods. **(A):** Similar results of X-gal staining were obtained in six independent experiments. **(B):** Data are expressed as the mean ± SD ($n = 3$). *, $p < .01$ **(C):** Either ES-EBs or iPS-EBs was transduced with Ad vectors by triple transduction (Triple) or by single transduction (Single). mCherry expression in ES-EBs or iPS-EBs was detected by confocal microscopy and flow cytometry. As a negative control, both types of EBs were transduced with Ad-null by triple transduction. Abbreviations: Ad, adenovirus; CA, cytomegalovirus enhancer/*β*-actin promoter; CMV, cytomegalovirus; EB, erythroid body; EF, elongation factor-1α; ES, embryonic stem; IPS, induced pluripotent stem; LacZ, *β*-galactosidase; RSV, Rous sarcoma virus.

characteristic of adipocyte differentiation (Fig. 4B, 4C). Interestingly, iPS cells were more efficiently differentiated into adipocytes than were ES cells after Ad vector transduction. The GPDH activity in PPARγ-transduced ES cells was two-fold higher than that in nontransduced or LacZ-transduced ES cells, whereas PPARγ-transduced iPS cells showed

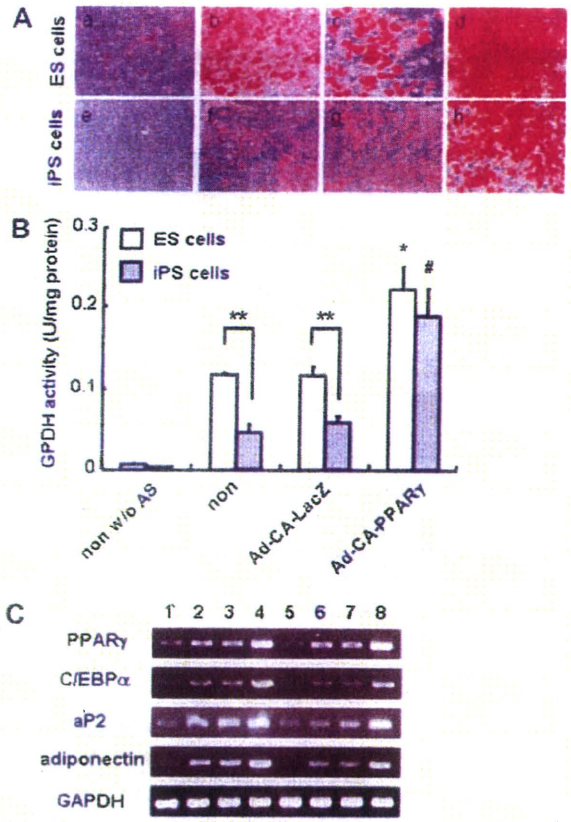

Figure 4. Efficient adipocyte differentiation from mouse ES cells and iPS cells by the transduction of the *PPARγ* gene. ES-EBs or iPS-EBs were transduced in triplicate with 10,000 vector particles/cell of Ad-CA-LacZ or Ad-CA-PPARγ. After plating onto a gelatin-coated dish on day 7, ES-EBs and iPS-EBs were cultured for 15 days in the presence or absence of AS. After cultivation, **(A)** lipid accumulation was detected by oil red O staining, and **(B)** GPDH activity in the cells was measured. **(A):** a, nontreated ES-EBs; b, ES-EBs with AS; c, ES-EBs with AS plus Ad-CA-LacZ; d, ES-EBs with AS plus Ad-CA-PPARγ; e, nontreated iPS-EBs; f, iPS-EBs with AS; g, iPS-EBs with AS plus Ad-CA-LacZ; h, iPS-EBs with AS plus Ad-CA-PPARγ. Scale bar = 60 μm. **(B):** Data are expressed as the mean ± SD (n = 3). * $p < .01$; ** $p < .05$, compared with nontransduced or Ad-CA-LacZ-transduced ES cells. #, $p < .05$, compared with nontransduced or Ad-CA-LacZ-transduced iPS cells. **(C):** Expression of PPARγ, C/EBPα, aP2, adiponectin, and GAPDH was measured by semiquantitative reverse transcriptase-polymerase chain reaction. Lane 1, nontreated ES-EBs; lane 2, ES-EBs with AS; lane 3, ES-EBs with AS plus Ad-CA-LacZ; lane 4, ES-EBs with AS plus Ad-CA-PPARγ; lane 5, nontreated iPS-EBs; lane 6, iPS-EBs with AS; lane 7, iPS-EBs with AS plus Ad-CA-LacZ; lane 8, iPS-EBs with AS plus Ad-CA-PPARγ. Abbreviations: AD, adenovirus; AS, adipogenic supplements; CA, cytomegalovirus enhancer/β-actin promoter; C/EBPα, CCAAT/enhancer binding protein α; ES, embryonic stem; EB, erythroid body; GAPDH, glyceraldehyde-3-phosphate dehydrogenase; GPDH, glycerol-3-phosphate dehydrogenase; IPS, induced pluripotent stem; LacZ, β-galactosidase; PPARγ, peroxisome proliferator-activated receptor γ; w/o, without.

approximately fourfold higher GPDH activity than nontransduced or LacZ-transduced iPS cells. These results showed that, like ES cells, iPS cells could be differentiated into adipocytes and that this adipocyte differentiation could be markedly facilitated by transient *PPARγ* gene transduction using an Ad vector.

Because Ad vector-mediated functional gene transduction was found to be effective to increase the differentiation efficiency from ES and iPS cells, we expected that other functional cells could be efficiently differentiated from ES and iPS cells by using an Ad vector. To confirm this finding, both types of cells were differentiated into osteoblasts by Ad vector-mediated transduction of a *Runx2* gene, which was previously proven to be indispensable for osteoblast differentiation [32, 33]. ES and iPS cells were transduced in triplicate with Ad-CA-LacZ or Ad-CA-Runx2 and were cultured with osteogenic supplements. We initially examined activity of ALP, an early osteoblast differentiation marker, in both types of cells, and showed that Ad-CA-Runx2-transduced cells exhibited higher ALP activity than nontransduced or Ad-CA-LacZ-transduced cells (Fig. 5A). These results indicated that early osteoblast differentiation was promoted by Ad vector-mediated *Runx2* gene transfer. Next, to estimate the mature osteoblast differentiation, matrix mineralization in the cells was detected by von Kossa staining. Consistent with the previous report [34], treatment with osteogenic supplements resulted in matrix mineralization in both types of cells, whereas in the absence of additives no calcification was observed (Fig. 5B). We also found that osteoblast differentiation from both ES and iPS cells could be dramatically promoted by Ad vector-mediated *Runx2* gene transduction (Fig. 5B). The level of calcium in Ad-CA-Runx2-transduced ES or iPS cells was approximately eightfold higher than that of nontransduced or Ad-CA-LacZ-transduced cells (Fig. 5C). Semiquantitative RT-PCR analysis also showed that the expression levels of Runx2, osterix, bone sialoprotein, osteocalcin, and type I collagen mRNA were up-regulated in the cells transduced with Ad-CA-Runx2 (Fig. 5D). These results demonstrated that the osteogenic potential in iPS cells was equal to that in ES cells and that efficient osteoblast differentiation from ES and iPS cells could be achieved by exogenous Runx2 expression using optimized Ad vectors.

Discussion

The establishment of an efficient gene transfer system for pluripotent cells would be quite useful for the application of these cells to regenerative medicine. We have previously developed suitable Ad vectors for transducing an exogenous gene into mouse ES cells and ES-EBs and showed that these Ad vectors could be successfully applied to regenerative medicine and basic studies [16, 17]. The aim of this study was to characterize the efficiency of transduction with Ad vectors in mouse iPS cells and to develop efficient methods for inducing the differentiation of mouse iPS cells by means of Ad vector transduction. This is the first study to report the detailed transduction properties of various types of Ad vectors in mouse iPS cells.

We optimized the transduction activity in mouse iPS cells and iPS-EBs by comparing four types of promoters (RSV, CMV, CA, and EF-1α) using Ad vectors. Because iPS cells have been shown to possess mostly the same properties as ES cells [4–6] and the CA and the EF-1α promoter exhibited strong transduction activity in mouse ES cells [16], we speculated that the same results might be obtained in mouse iPS cells. As we expected, mouse iPS cells and iPS-EBs were capable of being efficiently transduced by using a conventional Ad vector containing the CA (and the EF-1α) promoter (Figs. 2A, 3, supporting information Figs. S1, S2, S4). We found that a primary Ad receptor, CAR, was highly expressed in iPS cells (Fig. 1), which were generated from MEFs [4].

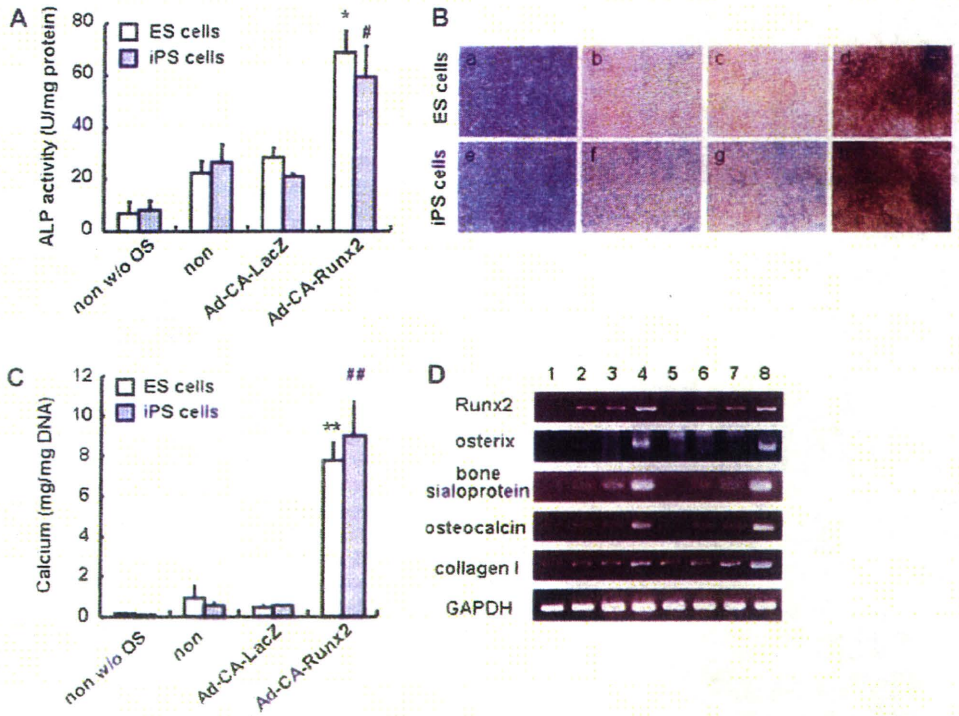

Figure 5. Enhanced osteoblast differentiation from ES cells and iPS cells in Ad-CA-Runx2-transduced cells. **(A):** ES-EBs or iPS-EBs were transduced in triplicate with 10,000 vector particles/cell of Ad-CA-LacZ or Ad-CA-Runx2. After culturing for 15 days with or without OS, ALP activity in the cells was determined. Data are expressed as the mean ± SD ($n = 3$). *, $p < .05$, compared with nontransduced or Ad-CA-LacZ-transduced ES cells. #, $p < .05$, compared with nontransduced or Ad-CA-LacZ-transduced iPS cells. Matrix mineralization in the cells was detected by von Kossa staining **(B)** and deposition of calcium was quantified as described in Materials and Methods **(C)**. **(B):** a, nontreated ES-EBs; b, ES-EBs with OS; c, ES-EBs with OS plus Ad-CA-LacZ; d, ES-EBs with OS plus Ad-CA-Runx2; e, nontreated iPS-EBs; f, iPS-EBs with OS; g, iPS-EBs with OS plus Ad-CA-LacZ; h, iPS-EBs with OS plus Ad-CA-Runx2. Scale bar = 60 μm. **(C):** Data are expressed as the mean ± SD ($n = 3$). **, $p < .01$, compared with nontransduced or Ad-CA-LacZ-transduced cells. ##, $p < .01$, compared with nontransduced or Ad-CA-LacZ-transduced iPS cells. **(D):** Total RNA was isolated, and semiquantitative reverse transcriptase-polymerase chain reaction was performed using primers for Runx2, osterix, bone sialoprotein, osteocalcin, collagen type I, and GAPDH. Lane 1, nontreated ES-EBs; lane 2, ES-EBs with OS; lane 3, ES-EBs with OS plus Ad-CA-LacZ; lane 4, ES-EBs with OS plus Ad-CA-Runx2; lane 5, nontreated iPS-EBs; lane 6, iPS-EBs with OS; lane 7, iPS-EBs with OS plus Ad-CA-LacZ; lane 8, iPS-EBs with OS plus Ad-CA-Runx2. Abbreviations: AD, adenovirus; ALP, alkaline phosphatase; CA, cytomegalovirus enhancer/β-actin promoter; ES, embryonic stem; EB, erythroid body; GAPDH, glyceraldehyde-3-phosphate dehydrogenase; IPS, induced pluripotent stem; LacZ, β-galactosidase; OS, osteogenic supplements; Runx2, runt-related transcription factor 2; w/o, without.

despite the low levels of CAR expression in MEFs [16]. This would lead to high transduction efficiency in mouse iPS cells when conventional Ad vectors containing the CA and the EF-1α promoter were used. In addition, we showed that more than 80% or 90% of the mouse iPS cells expressed mCherry after transduction with the Ad vector containing the CA promoter at 3,000 or 10,000 VPs/cell, respectively, without any decrease in the expression of pluripotent genes or viability (Fig. 2B–2D, 2F, supporting information Figs. 2, 3). Notably, Ad vector-transduced iPS cells still exhibited teratoma formation in vivo (Fig. 2E), and the efficiency of adipocyte or osteoblast differentiation in Ad-CA-LacZ-transduced iPS cells was similar to that in nontransduced iPS cells (Figs. 4, 5), indicating that Ad vector transduction did not change the pluripotency of iPS cells. These results indicate that gene transfer into mouse ES and iPS cells using an optimized conventional Ad vector would be useful for the application of these cells to both regenerative medicine and basic research.

We found that the CMV promoter, which is currently in wide use in transduction experiments, had weak activity in both mouse ES cells [16, 35] and mouse iPS cells (Fig. 2A, supporting information Fig. S1). Several groups have reported that undifferentiated ES cells expressed low levels of transgene when the CMV promoter was used, whereas the expression levels of reporter genes, when driven by the CMV promoter, were markedly increased in ES cell-derived neurons or cardiomyocytes [36, 37]. Consistent with our results (Fig. 3, supporting information Fig. S4), other authors have shown that the activity of the CMV promoter in ES-EBs was also lower than that of the CA and the EF-1α promoters [37]. These results suggest that the CMV promoter in the Ad vector would be silenced, possibly owing to DNA methylation [38] in mouse ES, ES-EB, and iPS cells. Interestingly, we observed that the CMV promoter was more strongly activated in mouse iPS-EBs than in ES-EBs (Fig. 3, supporting information Fig. S4). We have no idea why the CMV promoter was able to drive robust transgene expression in mouse iPS-EBs. It is possible that cellular types that comprise iPS-EBs might be different from those of ES-EBs because iPS cells showed slightly slower proliferation than ES cells (Fig. 2F) [4], which may have led to the difference in the transduction efficiency in iPS-EBs and ES-EBs when the CMV promoter was used. On the other hand, the expression levels of the three germ layer marker genes in iPS-EBs were largely comparable to those in ES-EBs (Fig. 1A), suggesting that, as for ES cells, iPS cells differentiate into ectoderm, mesoderm, and endoderm cells. Therefore, which kinds of cells in iPS-EBs

could express transgenes after the transduction with Ad vector containing the CMV promoter should be investigated. As with iPS-EBs, it has been reported that human ES cells and human ES cell-derived EBs, albeit not all ES cell clones, could also be transduced with an Ad vector containing the CMV promoter [39, 40]. Hence, further analysis of the precise mechanism regulating the CMV promoter in stem cells will be also needed.

We observed that mouse iPS cells could be differentiated into adipocytes and osteoblasts using the same protocols as those used for mouse ES cells (Figs. 4, 5). However, mouse iPS cells showed less efficient adipocyte differentiation than ES cells (Fig. 4), although almost no difference in osteoblast differentiation was observed between ES and iPS cells. *aP2* is a valuable indicator of adipocyte differentiation but there is no evidence that *aP2* is an adipocyte master gene (Fig. 4C). In addition, mouse iPS cells proliferated more slowly than ES cells as described above (Fig. 2F) [4], and thus their differentiation into adipocytes may have been delayed. To examine whether this is a general difference between ES and iPS cells or a specific characteristic of 20D17, we attempted to differentiate other iPS cell clones (38C2 and stm99-1) into adipocytes. Oil red O staining showed that the efficiency of adipocyte differentiation in 38C2-derived cells was equivalent to that in ES cell-derived cells, whereas stm99-1, like 20D17, had slightly less adipogenic potential than ES cells (supporting information Fig. S5). This result suggests that there is a difference in the differentiation potential among iPS cell clones. Therefore, to differentiate iPS cells into functional cells, the choice of appropriate iPS cell clone would be essential.

We showed that the efficiency of adipocyte differentiation from iPS cells was significantly increased by the triple transduction of the *PPARγ* gene (Fig. 4). We found previously that single transduction with Ad-CA-PPARγ into ES-EBs at day 5 was not enough for enhancing the adipocyte differentiation (our unpublished data). Although the transgene was not expressed in all of the cells that comprise ES-EBs or iPS-EBs even by triple transduction (Fig. 3C), transgene expression by at least triple transduction, but not by single transduction, should be necessary to trigger efficient differentiation. Thus, we concluded that gene transduction in triplicate into iPS cells would be required for promoting the differentiation of iPS cells into functional cells. Notably, PPARγ transduction in mouse iPS cells was more effective than that in mouse ES cells probably because the efficiency of Ad vector transduction was higher in mouse iPS cells than in mouse ES cells (Fig. 2C). Our data thus demonstrate that our transduction system can be successfully applied to mouse iPS cells. We also succeeded in efficient osteoblast differentiation from mouse ES cells and iPS cells by Ad vector-mediated Runx2 transduction. Previously, Tai et al. [41] reported that stable transduction of the *osterix* gene, which is required for osteoblastogenesis [42], in mouse ES cells promoted osteoblast differentiation. However, a *Runx2* gene transfer into either ES cells or iPS cells is considered to be more appropriate for differentiation into osteoblasts than an *osterix* gene, because Runx2 is necessary for mesenchymal cell differentiation toward mature osteoblasts [43] and osterix has been shown to function downstream of Runx2 [42]. Indeed, the expression levels of osterix mRNA were increased in Runx2-transduced cells (Fig. 5D). Furthermore, constitutive transgene expression might lead to undesirable effects, such as oncogenesis, after cellular differentiation. Therefore, we conclude that transient transduction of the *Runx2* gene into ES and iPS cells is preferable for efficient differentiation into osteoblasts and that our system could be a powerful tool to promote the cellular differentiation of mouse ES and iPS cells.

In summary, we developed an efficient gene delivery system for mouse iPS cells and demonstrated that this system is effective in promoting cellular differentiation. As for ES cells, mouse iPS cells could be differentiated into not only adipocytes and osteoblasts but also cardiomyocytes [44], cardiovascular cells [45], and hematopoietic cells [46], and iPS cells thus would be an ideal source of cells for regenerative medicine. More recently, it was demonstrated that mouse iPS cells could be generated by transduction of reprogrammed factors using Ad vectors [47] or nonviral vectors [48] and that the reprogrammed factors were not integrated in their genomes. Because these nonintegrated iPS cells also have the same characteristics as ES cells and reprogrammed factor-integrated iPS cells, our system would probably be applicable for nonintegrated iPS cells. Therefore, our transient expression system using Ad vectors could be a valuable tool for application to safer regenerative medicine using iPS cells.

Acknowledgments

We thank Dr. S. Yamanaka for kindly providing the mouse iPS cell lines 20D17, 38C2, and stm99-1. We also thank Dr. J. Miyazaki and Dr. T. Imai for providing the CA promoter and anti-mouse CAR monoclonal antibody, respectively. This work was supported by grants from the Ministry of Health, Labor, and Welfare of Japan. K.T. is a Research Fellow of the Japan Society for the Promotion of Science.

Disclosure of Potential Conflicts of Interest

The authors indicate no potential conflicts of interest.

References

1 Evans MJ, Kaufman MH. Establishment in culture of pluripotential cells from mouse embryos. Nature 1981;292:154–156.
2 Thomson JA, Itskovitz-Eldor J, Shapiro SS et al. Embryonic stem cell lines derived from human blastocysts. Science 1998;282: 1145–1147.
3 Takahashi K, Yamanaka S. Induction of pluripotent stem cells from mouse embryonic and adult fibroblast cultures by defined factors. Cell 2006;126:663–676.
4 Okita K, Ichisaka T, Yamanaka S. Generation of germline-competent induced pluripotent stem cells. Nature 2007;448:313–317.
5 Maherali N, Sridharan R, Xie W et al. Directly reprogrammed fibroblasts show global epigenetic remodeling and widespread tissue contribution. Cell Stem Cell 2007;1:55–70.
6 Wernig M, Meissner A, Foreman R et al. In vitro reprogramming of fibroblasts into a pluripotent ES-cell-like state. Nature 2007;448: 318–324.
7 Takahashi K, Tanabe K, Ohnuki M et al. Induction of pluripotent stem cells from adult human fibroblasts by defined factors. Cell 2007; 131:861–872.
8 Yu J, Vodyanik MA, Smuga-Otto K et al. Induced pluripotent stem cell lines derived from human somatic cells. Science 2007;318: 1917–1920.
9 Lowry WE, Richter L, Yachechko R et al. Generation of human induced pluripotent stem cells from dermal fibroblasts. Proc Natl Acad Sci UISIA 2008;105:2883–2888.
10 Park IH, Zhao R, West JA et al. Reprogramming of human somatic cells to pluripotency with defined factors. Nature 2008;451:141–146.
11 Kyba M, Perlingeiro RC, Daley GQ. HoxB4 confers definitive lymphoid-myeloid engraftment potential on embryonic stem cell and yolk sac hematopoietic progenitors. Cell 2002;109:29–37.

12 Liew CG, Shah NN, Briston SJ et al. PAX4 enhances β-cell differentiation of human embryonic stem cells. PLoS ONE 2008;3:e1783.
13 Chung S, Sonntag KC, Andersson T et al. Genetic engineering of mouse embryonic stem cells by Nurr1 enhances differentiation and maturation into dopaminergic neurons. Eur J Neurosci 2002;16: 1829–1838.
14 Kovesdi I, Brough DE, Bruder JT et al. Adenoviral vectors for gene transfer. Curr Opin Biotechnol 1997;8:583–589.
15 Benihoud K, Yeh P, Perricaudet M. Adenovirus vectors for gene delivery. Curr Opin Biotechnol 1999;10:440–447.
16 Kawabata K, Sakurai F, Yamaguchi T et al. Efficient gene transfer into mouse embryonic stem cells with adenovirus vectors. Mol Ther 2005;12:547–554.
17 Tashiro K, Kawabata K, Sakurai H et al. Efficient adenovirus vector-mediated PPAR gamma gene transfer into mouse embryoid bodies promotes adipocyte differentiation. J Gene Med 2008;10:498–507.
18 Tontonoz P, Hu E, Spiegelman BM. Stimulation of adipogenesis in fibroblasts by PPAR γ2, a lipid-activated transcription factor. Cell 1994;79:1147–1156.
19 Rosen ED, Sarraf P, Troy AE et al. PPARγ is required for the differentiation of adipose tissue in vivo and in vitro. Mol Cell 1999;4: 611–617.
20 Mizuguchi H, Kay MA. Efficient construction of a recombinant adenovirus vector by an improved in vitro ligation method. Hum Gene Ther 1998;9:2577–2583.
21 Mizuguchi H, Kay MA. A simple method for constructing E1- and E1/E4-deleted recombinant adenoviral vectors. Hum Gene Ther 1999; 10:2013–2017.
22 Niwa H, Yamamura K, Miyazaki J. Efficient selection for high-expression transfectants with a novel eukaryotic vector. Gene 1991; 108:193–199.
23 Sakurai H, Tashiro K, Kawabata K et al. Adenoviral expression of suppressor of cytokine signaling-1 reduces adenovirus vector-induced innate immune responses. J Immunol 2008;180:4931–4938.
24 Tashiro K, Kondo A, Kawabata K et al. Efficient osteoblast differentiation from mouse bone marrow stromal cells with polylysin-modified adenovirus vectors. Biochem Biophys Res Commun 2009;379: 127–132.
25 Maizel JV Jr, White DO, Scharff MD. The polypeptides of adenovirus. I. Evidence for multiple protein components in the virion and a comparison of types 2, 7A, and 12. Virology 1968;36:115–125.
26 Aoi T, Yae K, Nakagawa M et al. Generation of pluripotent stem cells from adult mouse liver and stomach cells. Science 2008;321:699–702.
27 Dani C, Smith AG, Dessolin S et al. Differentiation of embryonic stem cells into adipocytes in vitro. J Cell Sci 1997;110(Pt 11): 1279–1285.
28 Kawaguchi J, Mee PJ, Smith AG. Osteogenic and chondrogenic differentiation of embryonic stem cells in response to specific growth factors. Bone 2005;36:758–769.
29 Bergelson JM, Cunningham JA, Droguett G et al. Isolation of a common receptor for Coxsackie B viruses and adenoviruses 2 and 5. Science 1997;275:1320–1323.
30 Tomko RP, Xu R, Philipson L. HCAR and MCAR: the human and mouse cellular receptors for subgroup C adenoviruses and group B coxsackieviruses. Proc Natl Acad Sci USA 1997;94:3352–3356.
31 Mizuguchi H, Hayakawa T. Targeted adenovirus vectors. Hum Gene Ther 2004;15:1034–1044.
32 Ducy P, Zhang R, Geoffroy V et al. Osf2/Cbfa1: a transcriptional activator of osteoblast differentiation. Cell 1997;89:747–754.
33 Komori T, Yagi H, Nomura S et al. Targeted disruption of Cbfa1 results in a complete lack of bone formation owing to maturational arrest of osteoblasts. Cell 1997;89:755–764.
34 zur Nieden NI, Kempka G, Ahr HJ. In vitro differentiation of embryonic stem cells into mineralized osteoblasts. Differentiation 2003;71: 18–27.
35 Chung S, Andersson T, Sonntag KC et al. Analysis of different promoter systems for efficient transgene expression in mouse embryonic stem cell lines. Stem Cells 2002;20:139–145.
36 Rust EM, Westfall MV, Samuelson LC et al. Gene transfer into mouse embryonic stem cell-derived cardiac myocytes mediated by recombinant adenovirus. In Vitro Cell Dev Biol Anim 1997;33:270–276.
37 Hong S, Hwang DY, Yoon S et al. Functional analysis of various promoters in lentiviral vectors at different stages of in vitro differentiation of mouse embryonic stem cells. Mol Ther 2007;15: 1630–1639.
38 Brooks AR, Harkins RN, Wang P et al. Transcriptional silencing is associated with extensive methylation of the CMV promoter following adenoviral gene delivery to muscle. J Gene Med 2004;6: 395–404.
39 Rufaihah AJ, Haider HK, Heng BC et al. Directing endothelial differentiation of human embryonic stem cells via transduction with an adenoviral vector expressing the VEGF(165) gene. J Gene Med 2007; 9:452–461.
40 Brokhman I, Pomp O, Shaham L et al. Genetic modification of human embryonic stem cells with adenoviral vectors: differences of infectability between lines and correlation of infectability with expression of the coxsackie and adenovirus receptor. Stem Cells Dev 2009;18: 447–456.
41 Tai G, Polak JM, Bishop AE et al. Differentiation of osteoblasts from murine embryonic stem cells by overexpression of the transcriptional factor osterix. Tissue Eng 2004;10:1456–1466.
42 Nakashima K, Zhou X, Kunkel G et al. The novel zinc finger-containing transcription factor osterix is required for osteoblast differentiation and bone formation. Cell 2002;108:17–29.
43 Marie PJ. Transcription factors controlling osteoblastogenesis. Arch Biochem Biophys 2008;473:98–105.
44 Mauritz C, Schwanke K, Reppel M et al. Generation of functional murine cardiac myocytes from induced pluripotent stem cells. Circulation 2008;118:507–517.
45 Narazaki G, Uosaki H, Teranishi M et al. Directed and systematic differentiation of cardiovascular cells from mouse induced pluripotent stem cells. Circulation 2008;118:498–506.
46 Schenke-Layland K, Rhodes KE, Angelis E et al. Reprogrammed mouse fibroblasts differentiate into cells of the cardiovascular and hematopoietic lineages. Stem Cells 2008;26:1537–1546.
47 Stadtfeld M, Nagaya M, Utikal J et al. Induced pluripotent stem cells generated without viral integration. Science 2008;322:945–949.
48 Okita K, Nakagawa M, Hyenjong H et al. Generation of mouse induced pluripotent stem cells without viral vectors. Science 2008; 322:949–953.


See www.StemCells.com for supporting information available online.

Biochemical and Biophysical Research Communications 379 (2009) 127–132

Contents lists available at ScienceDirect

Biochemical and Biophysical Research Communications

journal homepage: www.elsevier.com/locate/ybbrc

Efficient osteoblast differentiation from mouse bone marrow stromal cells with polylysin-modified adenovirus vectors

Katsuhisa Tashiro [a,b], Asami Kondo [a], Kenji Kawabata [a], Haruna Sakurai [a,b], Fuminori Sakurai [a], Koichi Yamanishi [b,c], Takao Hayakawa [d,e], Hiroyuki Mizuguchi [a,b,*]

[a] Laboratory of Gene Transfer and Regulation, National Institute of Biomedical Innovation, 7-6-8 Saito-Asagi, Ibaraki, Osaka 567-0085, Japan
[b] Graduate School of Pharmaceutical Sciences, Osaka University, 1-6 Yamadaoka, Suita, Osaka 565-0871, Japan
[c] National Institute of Biomedical Innovation, 7-6-8 Saito-Asagi, Ibaraki, Osaka 567-0085, Japan
[d] Pharmaceutics and Medical Devices Agency, 3-3-2, Kasumigaseki, Chiyoda-Ku, Tokyo 100-0013, Japan
[e] Pharmaceutical Research and Technology Institute, Kinki University, 3-4-1. Kowakae, Higashi-Osaka, Osaka 577-8502, Japan

ARTICLE INFO

Article history:
Received 2 December 2008
Available online 25 December 2008

Keywords:
Fiber-modified adenovirus vectors
Bone marrow stromal cells
Osteoblasts

ABSTRACT

Bone marrow stromal cells (BMSCs) are expected to be a source for tissue regeneration because they can differentiate into multiple cell types. Establishment of efficient gene transfer systems for BMSCs is essential for their application to regenerative medicine. In this study, we compared the transduction efficiency in mouse primary BMSCs by using fiber-modified adenovirus (Ad) vectors, and demonstrated that AdK7, which harbors a polylysin (K7) peptide in the C-terminus of the fiber knob, could efficiently express a transgene in BMSCs. Notably, AdK7 robustly drove transgene expression in more than 90% of the BMSCs at 3,000 vector particles/cell. Furthermore, we showed that *in vitro* and *in vivo* osteogenic potential of BMSCs was dramatically promoted by the transduction of Runx2 gene using AdK7. These results indicate that this transduction system could be a powerful tool for therapeutic applications based on BMSCs.

Because bone marrow stromal cells (BMSCs) containing mesenchymal stem cells (MSCs) can be easily isolated from adult tissues and efficiently expanded *in vitro*, and can differentiate into multiple cell types [1,2], BMSCs are expected to be an ideal source of cells for the regeneration of tissues. However, it is difficult to obtain a large amount of pure differentiated cells from BMSCs because of their low differentiation efficiency. The cell transition from stem cells to lineage-committed cells involves many transcription factors that promote or suppress cellular differentiation [3]. Thus, to develop an efficient method for differentiating from BMSCs into specialized cells, we planned to combine the transduction of a functional gene, which promotes cellular differentiation, with stimulation by chemical reagents. To do this procedure, it is essential to develop efficient transduction systems for BMSCs.

Among the various types of gene delivery vectors, adenovirus (Ad) vectors have been widely used for gene transfer studies, since they can achieve high transduction efficiency and transduce both dividing and non-dividing cells [4]. Although Ad vector-mediated transduction into BMSCs has been performed, the transduction efficiency was found to be lower than those of many other cell lines [5,6]. This is due to the low levels of coxsackievirus and adenovirus receptor (CAR), which mediates adenovirus entry, on the cell surface [5,6]. To overcome this problem, we and others have generated several types of fiber-modified Ad vectors, which mediate efficient gene transduction into the cells expressing very low levels of CAR [7,8]. Transduction efficiency was improved in various types of the cells by the insertion of Arg-Gly-Asp (RGD) peptide or 7-tandem lysine residues (KKKKKKK: K7) peptide, which targets αv integrins or heparan sulfates, respectively, on the cell surface, into the fiber knob of the Ad vector [7,8]. In particular, we previously reported that polylysin-modified Ad vector (AdK7) is the most suitable vector for transduction into human bone marrow-derived MSCs (hMSCs) [9].

In this study, we initially investigated the transduction efficiency of mouse primary BMSCs by using fiber-modified Ad vectors. We next examined whether the osteogenic potential of BMSCs was promoted by using Ad vector-mediated transduction of a runt-related transcription factor 2 (Runx2) gene, which is known as a master gene for osteoblastogenesis [10,11].

Materials and methods

Ad vectors. Ad vectors were constructed using an improved *in vitro* ligation method [12,13]. The CA (cytomegalovirus (CMV) enhancer/β-actin promoter) promoter [14]-driven β-galactosidase

* Corresponding author. Address: Laboratory of Gene Transfer and Regulation, National Institute of Biomedical Innovation, 7-6-8 Saito-Asagi, Ibaraki, Osaka 567-0085, Japan. Fax: +81 72 641 9816.
E-mail address: mizuguch@nibio.go.jp (H. Mizuguchi).

0006-291X/$ - see front matter © 2008 Elsevier Inc. All rights reserved.
doi:10.1016/j.bbrc.2008.12.055

(LacZ)-expressing plasmid, pHMCA-LacZ [15], was digested with I-*CeuI*/PI-*SceI* and inserted into I-*CeuI*/PI-*SceI*-digested pAdHM15-RGD [16] or pAdHM41-K7 (C) [8], resulting in pAdRGD-CA-LacZ, pAdK7-CA-LacZ, respectively. The CMV or the human elongation factor (EF)-1α promoter-driven LacZ-expressing plasmid, pHMCMV-LacZ [15] or pHMEF-LacZ [15], respectively, was also digested with I-*CeuI*/PI-*SceI* and ligated into I-*CeuI*/PI-*SceI*-digested-pAdHM41-K7 (C), resulting in pAdK7-CMV-LacZ or pAdK7-EF-LacZ, respectively. The CA promoter-driven mouse Runx2-expressing plasmid, pHMCA-Runx2, was generated by inserting a mouse Runx2 cDNA, which is derived from pCMV-Runx2 (a kind gift from Dr. S. Takeda, Tokyo Medical and Dental University, Tokyo, Japan) [17], into pHMCA5. pHMCA-Runx2 was also digested with I-*CeuI*/PI-*SceI*, and inserted with pAdHM4 [12] or pAdHM41-K7 (C), resulting in pAd-CA-Runx2 or pAdK7-CA-Runx2, respectively. Ad vectors (Ad-CA-LacZ, AdRGD-CA-LacZ, AdK7-CA-LacZ, AdK7-CMV-LacZ, AdK7-EF-LacZ, Ad-CA-Runx2, and AdK7-CA-Runx2) were generated and purified as described previously [18]. Determination of virus particle (VP) and biological titer were determined using by a spectrophotometrical method [19] and by means of an Adeno-X Rapid Titer Kit (Clontech, Palo Alto, CA), respectively. The ratio of the biological-to-particle titer was 1:14 for Ad-CA-LacZ, 1:35 for AdRGD-CA-LacZ, 1:42 for AdK7-CA-LacZ, 1:25 for AdK7-CMV-LacZ, 1:32 for AdK7-EF-LacZ, 1:17 for Ad-CA-Runx2, and 1:28 for AdK7-CA-Runx2.

Mouse primary BMSCs. Primary BMSCs were harvested from female C57BL/6 mice (8 weeks; Nippon SLC, Shizuoka, Japan) as below. Femora and tibias were isolated and placed in Dulbecco's modified Eagle's medium (DMEM; Sigma, St. Louis, MO)/20% fetal bovine serum (FBS; Invitrogen, Carlsbad, CA) and 1% penicillin/streptomycin. Bone marrow was obtained by flushing these bones, and cells recovered from the bones of one animal were then seeded into a 150 mm tissue culture plate. Medium was changed every 2 days to remove non-adherent cells, and adherent cells were cultured until reaching confluence. At confluence, BMSCs were passaged after digestion with 0.25% trypsin/1 mM EDTA. BMSCs (passage 4–12) were subsequently used for further analysis.

LacZ assay. BMSCs (1×10^4 cells) were plated in 24-well plates. The next day, they were transduced with the indicated doses of Ad vectors for 1.5 hr. Two days later, X-gal staining and β-gal luminescence assays were performed as described previously [18].

Osteoblasts differentiation. BMSCs (1×10^4 cells) were plated in 24-well plates. Cells were transduced with 3000 VP/cell of Ad vector for 1.5 hr. After aspirating the viral solution, osteogenic differentiation medium, consisting of growth medium (DMEM/20% FBS) containing 50 μg/mL ascorbic acid 2-phosphate (Sigma), 5 mM β-glycerophosphate (Sigma), and 100 nM dexamethasone (Wako, Osaka, Japan), was added. The medium was replaced every 3 days.

von Kossa staining, calcium quantitation. Cells were fixed with 4% paraformaldehyde/phosphate-buffered saline (PBS) and stained with $AgNO_3$ by the von Kossa method. To measure calcium deposition, cells were washed twice with PBS and decalcified with 0.5 M acetic acid, and cell culture plates were rotated overnight at room temperature (R/T). Insoluble material was removed by centrifugation. The supernatants were then assayed for calcium with the calcium C-test Wako kit (Wako). DNA in pellets was extracted using the DNeasy tissue kit (Qiagen), and calcium content was then normalized to DNA.

ALP assay. Cells were lysed in 10 mM Tris–HCl (pH 7.5) containing 1 mM $MgCl_2$ and 0.1% Triton X-100, and the lysates were then used for assay. Alkaline phosphatase (ALP) activity was measured using the LabAssay ALP kit (Wako) according to the manufacturer's instructions. The protein concentration of the lysates was determined using a Bio-Rad assay kit (Bio-Rad laboratories, Hercules, CA), and ALP activity was then normalized by protein concentration.

RT-PCR. RT-PCR was performed as described previously [18]. The sequences of primers were as follows: Runx2(F), 5′-CCT CTG ACT TCT GCC TCT GG-3′; Runx2(R), 5′-CAG CGT CAA CAC CAT CAT TC-3′; osterix(F), 5′- CTT AAC CCA GCT CCC TAC CC-3′; osterix(R), 5′- TGT GAA TGG GCT TCT TCC TC-3′; bone sialoprotein(F), 5′- AAA GTG AAG GAA AGC GAC GA-3′; bone sialoprotein(R), 5′-GTT CCT TCT GCA CCT GCT TC-3′; osteocalcin(F), 5′-GCG CTC TGT CTC TCT GAC CT -3′; osteocalcin(R), 5′-TTT GTA GGC GGT CTT CAA GC-3′; collagen Iα1(F), 5′-CAC CCT CAA GAG CCT GAG TC-3′; collagen Iα1 (R), 5′-GCT ACG CTG TTC TTG CAG TG-3′, GAPDH(F), 5′-ACC ACA GTC CAT GCC ATC AC-3′; GAPDH(R), 5′-TCC ACC ACC CTG TTG CTG TA-3′.

Western blotting. Western blotting was performed as described previously [18]. Briefly, lysates (20 μg) were subjected to 12.5% polyacrylamide gel and were transferred to a polyvinylidene fluoride membrane (Millipore, Bedford, MA). After blocking with Immunoblock (DS Pharma Biomedical, Osaka, Japan) at R/T for 1 hr, the membrane was exposed to rabbit anti-Runx2 antibody (Santa Cruz Biotechnology, Inc., Santa Cruz, CA) at 4 °C overnight, followed by horseradish peroxidase-conjugated secondary antibody at R/T for 1 hr. The band was visualized by ECL Plus Western blotting detection reagents (Amersham Bioscience, Piscataway, NJ) and the signals were read using a LAS-3000 imaging system (FUJIFILM, Tokyo, Japan). All blots were stripped and reblotted with antibody against β-actin (Sigma) for normalization.

In vivo heterotopic bone formation. BMSCs (2×10^6 cells, passage 8–9) were transduced with AdK7-CA-LacZ, AdK7-CA-Runx2, or Ad-CA-Runx2, at 3000 VP/cells for 1.5 hr. The next day, cells were collected by trypsin, and resuspended in 150 μl of PBS, and then injected into the hind limb biceps muscle of nude mice (Nippon SLC) (2animal/ group). At 4–5 weeks after injection, mice were anesthetized by isofluorane and bone formation was analyzed with a microcomputed tomography (microCT) system (eXplore Locus CT System; GE Healthcare, London, ON, Canada). Both an X-ray image and a three-dimensional reconstitution image were obtained by using the microCT system.

Results

Optimization of transduction efficiency in BMSCs by using various types of Ad vectors

To optimize Ad vectors for transduction into BMSCs, we prepared three LacZ-expressing Ad vectors, Ad-CA-LacZ, AdRGD-CA-LacZ, and AdK7-CA-LacZ. We investigated the transduction efficiency of these Ad vectors in BMSCs at the indicated vector dose. X-gal staining showed that LacZ-positive cells were less than 10% even at a dose of 3000 vector particles (VP)/cell in Ad-CA-LacZ (Fig. 1A). On the other hand, more than 90% of the cells expressed LacZ at the same dose in AdK7-CA-LacZ. A luminescence assay revealed that, at 3000 VP/cell, the LacZ expression level in the cells transduced with AdRGD-CA-LacZ or AdK7-CA-LacZ was increased by about 5- or 50-fold, respectively, in comparison with that in the cells transduced with Ad-CA-LacZ (Fig. 1B). These results were quite similar to those of our previous report, in which efficient transduction in hMSCs was achieved by using AdK7 [9], and our data clearly demonstrated that AdK7 is a suitable vector for transduction into both mouse BMSCs and hMSCs.

We and others reported that the choice of promoters is important for transduction efficiency, especially in immature cells [15,18,20,21]. Thus, we examined the transduction efficiency by comparing the promoter activities in BMSCs. In addition to the CA promoter, we prepared LacZ-expressing AdK7 under the control of the CMV promoter or the EF-1α promoter (AdK7-CMV-LacZ or AdK7-EF-LacZ, respectively). A luminescent assay showed that the CA promoter represented the highest transgene expression

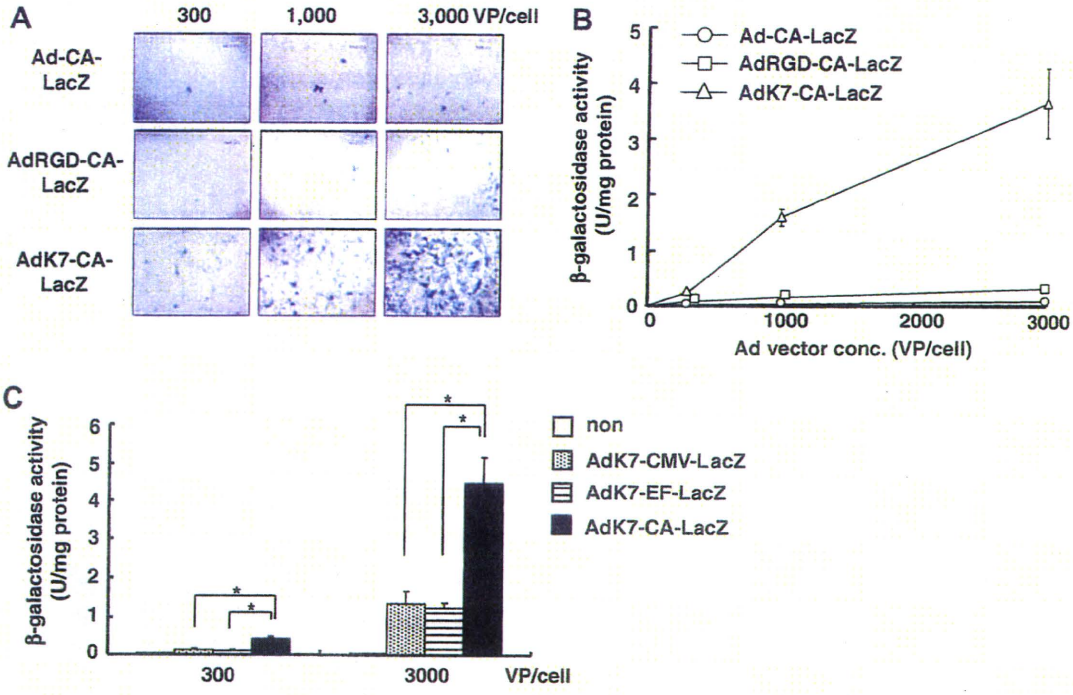

Fig. 1. Gene transduction efficiency in mouse primary BMSCs by various types of Ad vectors. Mouse BMSCs were transduced with the indicated doses of LacZ-expressing Ad vectors. Two days later, (A) X-gal staining and (B) luminescence assay were performed. Similar results of X-gal staining were obtained in three independent experiments. Scale bar indicates 200 μm. (C) Optimization of promoter activity in BMSCs using LacZ-expressing AdK7. BMSCs were transduced with the indicated dose of each Ad vector, and LacZ expression in the cells was measured. The data are expressed as mean ± S.D. ($n = 3$). $p < 0.01$.

among the three types of the promoters (Fig. 1C). These results demonstrate that AdK7 containing the CA promoter is the most effective at attaining high transduction efficiency in mouse BMSCs.

We also investigated the cytotoxicity in BMSCs transduced with AdK7-CA-LacZ. Almost no difference in cell number between non-transduced cells and AdK7-CA-LacZ-transduced cells was observed on day 2 after transduction (data not shown), indicating that AdK7 is an excellent vector with high transduction activity and low cytotoxicity in BMSCs.

Efficient osteoblast differentiation in vitro and in vivo by fiber-modified Ad vectors

Because an efficient method for transduction into BMSCs could be established by using AdK7 containing the CA promoter, we expected that efficient differentiation into specialized cells from BMSCs might be achieved by using this Ad vector. To test this, we generated mouse Runx2-expressing Ad vectors, AdK7-CA-Runx2 and Ad-CA-Runx2, because a Runx2 gene is both necessary and sufficient for mesenchymal cell differentiation towards osteoblast lineage [3]. Western blot analysis showed that Runx2 protein levels in AdK7-CA-Runx2-transduced cells were quite higher than those in non-, AdK7-CA-LacZ-, or Ad-CA-Runx2-transduced cells (Fig. 2).

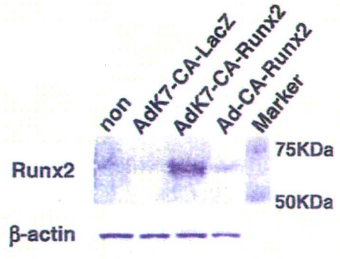

Fig. 2. Runx2 expression in Ad vector-transduced BMSCs. Cell lysates were isolated from BMSCs 2 days after the transduction, and Western blotting was performed.

We next assessed osteoblast differentiation by measuring alkaline phosphatase (ALP) activity, which is a marker of early osteoblast differentiation. After transduction with Ad vector, BMSCs were cultured in osteogenic differentiation medium for the indicated number of days. As shown in Fig. 3A, the ALP activity levels in AdK7-CA-Runx2-transduced cells were extremely increased in comparison with control cells. Notably, AdK7-CA-Runx2 mediated approximately 50-fold higher ALP activity than non-transduction or AdK7-CA-LacZ on day 5 after transduction. These results indicated that early osteoblast differentiation of BMSC was facilitated by AdK7-CA-Runx2. Because mature osteoblasts are known to be specialized in the production of extracellular matrix and the mineralization [22], we next examined the matrix mineralization in BMSCs. von Kossa staining revealed that matrix mineralization in AdK7-CA-Runx2-transduced cells was dramatically increased in comparison with non-, AdK7-CA-LacZ, or Ad-CA-Runx2-transduced cells (Fig. 3B, left). Furthermore, we observed a significant elevation of calcium deposition in AdK7-CA-Runx2-transduced cells even on day 5 after transduction, while neither non-transduced cells nor AdK7-CA-LacZ-transduced cells showed mineralization until day 15 (Fig. 3B, right). Ad-CA-Runx2 mediated slightly higher levels of calcium deposition than non-transduced or AdK7-CA-LacZ-transduced cells, but significantly lower levels than AdK7-CA-Runx2-transduced cells. Additionally, we found that the expression levels of marker genes characteristic of osteoblast differentiation, such as Runx2, osterix, bone sialoprotein, osteocalcin, and type I collagen, were also increased in AdK7-CA-Runx2-transduced cells (Fig. 3C). These results demonstrated that a conventional method using only osteogenic differentiation medium is

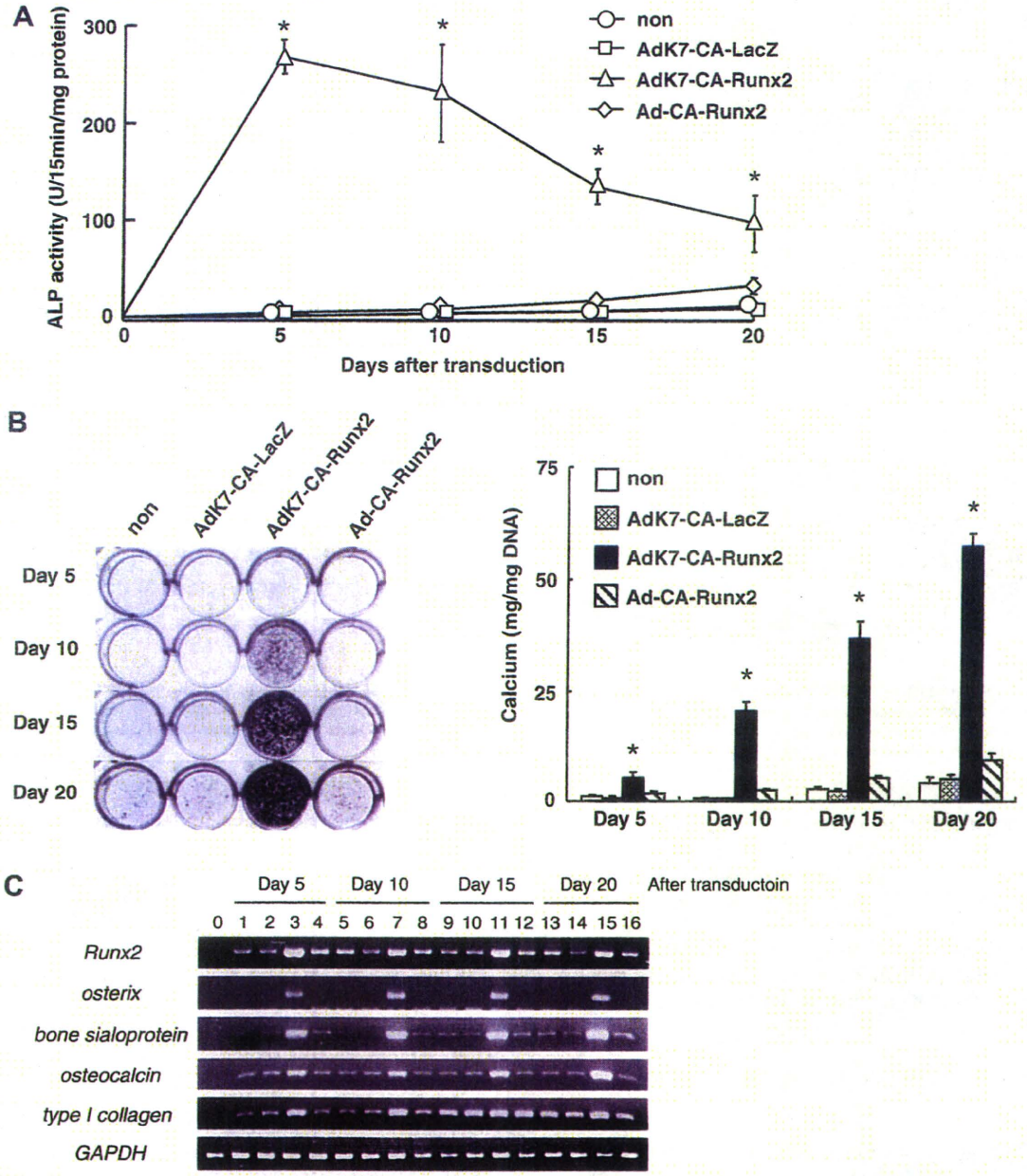

Fig. 3. Promotion of *in vitro* osteoblastic differentiation in AdK7-CA-Runx2-transduced BMSC. After transduction with each Ad vector at 3000 VP/cell for 1.5 hr, BMSCs were cultured for the indicated number of days. (A) ALP activity, (B, left) matrix mineralization, and (B, right) calcium deposition in the cells was determined. The data are expressed as mean ± S.D. ($n = 3$). * $p < 0.01$ as compared with non-, AdK7-CA-LacZ-, or Ad-CA-Runx2-transduced cells. (C) RT-PCR was performed using primers for Runx2, osterix, bone sialoprotein, osteocalcin, collagen type I, and GAPDH. Lane 0: non-treated BMSCs; lanes 1, 5, 9, and 13: BMSCs with osteogenic supplements (OS); lanes 2, 6, 10, and 14: BMSCs with OS plus AdK7-CA-LacZ; lanes 3, 7, 11, and 15: BMSCs with OS plus AdK7-CA-Runx2; lanes 4, 8, 12, and 16: BMSCs with OS plus Ad-CA-Runx2.

not enough for efficient osteoblast differentiation, and that, by efficient Runx2 transduction using AdK7, osteoblastogenesis of BMSCs could be dramatically accelerated *in vitro*.

Finally, to examine whether the increased levels of Runx2 expression in BMSCs could enhance the osteogenic potential of BMSC *in vivo*, BMSCs transduced with each Ad vector were injected into the hind limb biceps muscle of nude mice. Microcomputed tomography analysis revealed that no bone formation was observed in non-, AdK7-CA-LacZ-, or Ad-CA-Runx2-transduced cells, while new bone was detected in mice injected with AdK7-CA-Runx2-transduced cells (Fig. 4), indicating that AdK7-CA-Runx2-transduced BMSCs efficiently differentiated into mature osteoblasts *in vivo*. These results clearly showed that AdK7-CA-Runx2 could facilitate the osteogenic potential of BMSCs both *in vitro* and *in vivo*.

Discussion

Because genetic manipulation is considered to be a powerful tool to promote cellular differentiation, it is necessary to establish efficient methods for transduction into BMSCs. Many researchers have reported that transduction efficiency of rat or human MSC was increased by using fiber-modified Ad vectors, such as AdRGD or Ad vectors containing Ad35 fiber knob and

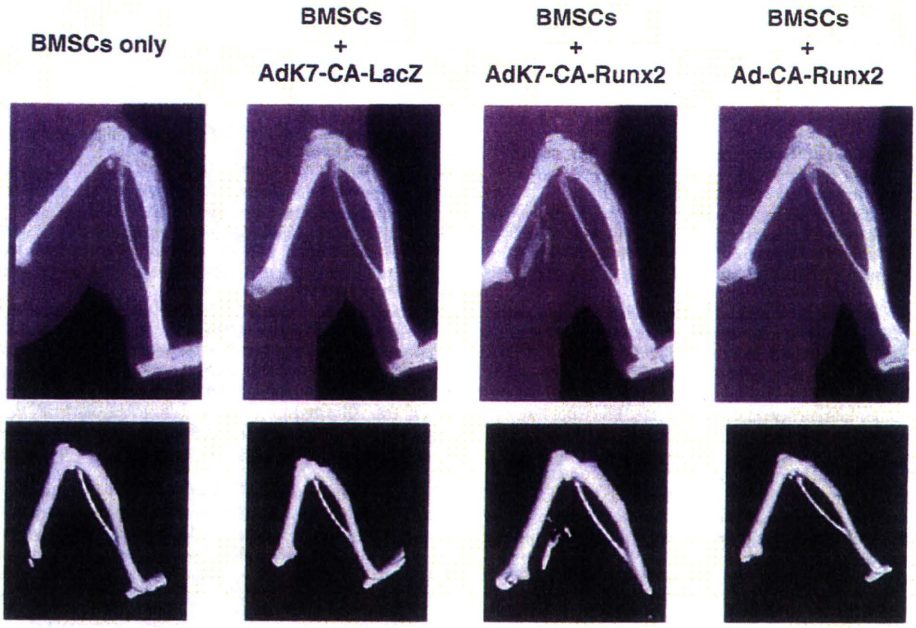

Fig. 4. *In vivo* ectopic bone formation of mouse BMSCs by AdK7-mediated Runx2 gene transduction. BMSCs were transduced with indicated Ad vectors at 3000 VP/cell. On the following day, cells were injected into the hind limb biceps muscle of nude mice. Four weeks later, bone formation was analyzed by the microCT system. Similar results were obtained in two independent experiments. Upper: X-ray images; lower: 3D reconstitution images.

shaft (AdF35) [23–25]. In this study, we demonstrated that AdK7 could express a transgene in BMSCs more efficiently than conventional Ad vector or AdRGD (Fig. 1A and B). Similarly, we have previously shown that the highest transduction efficiency in hMSC could be achieved by using AdK7, but not AdRGD or AdF35 [9]. Therefore, our data indicate that AdK7 is the most appropriate vector for various mesenchymal cells. We also found that the CA promoter showed higher gene expression in BMSCs than did the CMV or EF-1α promoter (Fig. 1C). This appears to be due to the potent activity of the CA promoter in immature cells [18,20]. Hence, we conclude that AdK7 containing the CA promoter is the most suitable vector for transduction into BMSCs.

We demonstrated that osteoblastogenesis of BMSCs was dramatically promoted by using AdK7-mediated Runx2 transduction (Figs. 3 and 4). This is the first study to report the usefulness of AdK7 in the field of stem cell differentiation. Runx2 is known to regulate osteoblastogenesis by controlling the expression of multiple osteoblast marker genes [10]. Because Runx2 protein and mRNA were highly expressed for more than 20 days in AdK7-CA-Runx2-trasduced cells (Figs. 2 and 3C), the expression of marker genes and ALP activity would be increased and would thereby enhance both *in vitro* and *in vivo* osteogenic ability. On the other hand, osteoblast differentiation could not be facilitated by AdK7-CA-Runx2 when osteogenic supplements were removed (data not shown), suggesting that osteogenic supplements were required for matrix mineralization, although differentiation efficiency was low when using only osteogenic supplements. Thus, efficient osteoblast differentiation of BMSCs would be achieved by the synergistic effect of both osteogenic supplements and efficient Runx2 transduction.

Unlike the case with AdK7-CA-Runx2, almost no osteoblast differentiation was seen in Ad-CA-Runx2-transduced cells. However, several groups reported that the osteogenic potential of MSCs was enhanced by Runx2 transduction using the conventional Ad vectors [26,27]. This difference would be attributable to the difference in transduction efficiency in BMSCs using the conventional Ad vector, because they showed that approximately 30–40% of the cells expressed transgenes by conventional Ad vector at 250–500 infectious units (ifu)/cell. Although we could not obtain high transduction efficiency using the conventional Ad vector, we showed that more than 90% of the cells were transduced by using AdK7-CA-LacZ at only 71 ifu/cell (3000 VP/cell) (Fig. 1A), without any decrease in viability (data not shown). Our results indicate that vector doses can be reduced by using AdK7, leading to a decrease in cytotoxicity to the cells. Therefore, AdK7, but not other fiber-modified Ad vectors or conventional Ad vectors, would contribute to safe regenerative medicine procedures.

In summary, we succeeded in developing efficient methods both for transducing mouse BMSCs and differentiating osteoblasts from BMSCs. Recently, many researchers have reported that mesenchymal stem/stromal cells could be isolated from adipose or placental tissues [28,29]. Because these mesenchymal cells are shown to possess mostly the same properties as BMSCs, AdK7 could probably be applied to these cells. Thus, our transduction methods can be a valuable tool for therapeutic applications based on adult mesenchymal stem/stromal cells.

Acknowledgments

We thank Dr. J. Miyazaki and Dr. S. Takeda for providing the CA promoter and the mouse Runx2 cDNA, respectively. This work was supported by grants from the Ministry of Health, Labor, and Welfare of Japan. K.T. is the Research Fellow of the Japan Society for the Promotion of Science.

References

[1] M.F. Pittenger, A.M. Mackay, S.C. Beck, R.K. Jaiswal, R. Douglas, J.D. Mosca, M.A. Moorman, D.W. Simonetti, S. Craig, D.R. Marshak, Multilineage potential of adult human mesenchymal stem cells, Science 284 (1999) 143–147.
[2] M.F. Pittenger, B.J. Martin, Mesenchymal stem cells and their potential as cardiac therapeutics, Circ. Res. 95 (2004) 9–20.

[3] P.J. Marie, Transcription factors controlling osteoblastogenesis, Arch. Biochem. Biophys. 473 (2008) 98–105.
[4] K. Benihoud, P. Yeh, M. Perricaudet, Adenovirus vectors for gene delivery, Curr. Opin. Biotechnol. 10 (1999) 440–447.
[5] P.A. Conget, J.J. Minguell, Adenoviral-mediated gene transfer into ex vivo expanded human bone marrow mesenchymal progenitor cells, Exp. Hematol. 28 (2000) 382–390.
[6] S.C. Hung, C.Y. Lu, S.K. Shyue, H.C. Liu, L.L. Ho, Lineage differentiation-associated loss of adenoviral susceptibility and coxsackie-adenovirus receptor expression in human mesenchymal stem cells, Stem cells 22 (2004) 1321–1329.
[7] I. Dmitriev, V. Krasnykh, C.R. Miller, M. Wang, E. Kashentseva, G. Mikheeva, N. Belousova, D.T. Curiel, An adenovirus vector with genetically modified fibers demonstrates expanded tropism via utilization of a coxsackievirus and adenovirus receptor-independent cell entry mechanism, J. Virol. 72 (1998) 9706–9713.
[8] N. Koizumi, H. Mizuguchi, N. Utoguchi, Y. Watanabe, T. Hayakawa, Generation of fiber-modified adenovirus vectors containing heterologous peptides in both the HI loop and C terminus of the fiber knob, J. Gene Med. 5 (2003) 267–276.
[9] H. Mizuguchi, T. Sasaki, K. Kawabata, F. Sakurai, T. Hayakawa, Fiber-modified adenovirus vectors mediate efficient gene transfer into undifferentiated and adipogenic-differentiated human mesenchymal stem cells, Biochem. Biophys. Res. Commun. 332 (2005) 1101–1106.
[10] P. Ducy, R. Zhang, V. Geoffroy, A.L. Ridall, G. Karsenty, Osf2/Cbfa1: a transcriptional activator of osteoblast differentiation, Cell 89 (1997) 747–754.
[11] T. Komori, H. Yagi, S. Nomura, A. Yamaguchi, K. Sasaki, K. Deguchi, Y. Shimizu, R.T. Bronson, Y.H. Gao, M. Inada, M. Sato, R. Okamoto, Y. Kitamura, S. Yoshiki, T. Kishimoto, Targeted disruption of Cbfa1 results in a complete lack of bone formation owing to maturational arrest of osteoblasts, Cell 89 (1997) 755–764.
[12] H. Mizuguchi, M.A. Kay, Efficient construction of a recombinant adenovirus vector by an improved in vitro ligation method, Hum. Gene Ther. 9 (1998) 2577–2583.
[13] H. Mizuguchi, M.A. Kay, A simple method for constructing E1- and E1/E4-deleted recombinant adenoviral vectors, Hum. Gene Ther. 10 (1999) 2013–2017.
[14] H. Niwa, K. Yamamura, J. Miyazaki, Efficient selection for high-expression transfectants with a novel eukaryotic vector, Gene 108 (1991) 193–199.
[15] K. Kawabata, F. Sakurai, T. Yamaguchi, T. Hayakawa, H. Mizuguchi, Efficient gene transfer into mouse embryonic stem cells with adenovirus vectors, Mol. Ther. 12 (2005) 547–554.
[16] H. Mizuguchi, N. Koizumi, T. Hosono, N. Utoguchi, Y. Watanabe, M.A. Kay, T. Hayakawa, A simplified system for constructing recombinant adenoviral vectors containing heterologous peptides in the HI loop of their fiber knob, Gene Ther. 8 (2001) 730–735.
[17] S. Takeda, J.P. Bonnamy, M.J. Owen, P. Ducy, G. Karsenty, Continuous expression of Cbfa1 in nonhypertrophic chondrocytes uncovers its ability to induce hypertrophic chondrocyte differentiation and partially rescues Cbfa1-deficient mice, Genes Dev. 15 (2001) 467–481.
[18] K. Tashiro, K. Kawabata, H. Sakurai, S. Kurachi, F. Sakurai, K. Yamanishi, H. Mizuguchi, Efficient adenovirus vector-mediated PPAR gamma gene transfer into mouse embryoid bodies promotes adipocyte differentiation, J. Gene Med. 10 (2008) 498–507.
[19] J.V. Maizel Jr., D.O. White, M.D. Scharff, The polypeptides of adenovirus. I. Evidence for multiple protein components in the virion and a comparison of types 2, 7A, and 12, Virology 36 (1968) 115–125.
[20] F. Sakurai, K. Kawabata, T. Yamaguchi, T. Hayakawa, H. Mizuguchi, Optimization of adenovirus serotype 35 vectors for efficient transduction in human hematopoietic progenitors: comparison of promoter activities, Gene Ther. 12 (2005) 1424–1433.
[21] S. Chung, T. Andersson, K.C. Sonntag, L. Bjorklund, O. Isacson, K.S. Kim, Analysis of different promoter systems for efficient transgene expression in mouse embryonic stem cell lines, Stem Cells 20 (2002) 139–145.
[22] H.C. Blair, M. Zaidi, P.H. Schlesinger, Mechanisms balancing skeletal matrix synthesis and degradation, Biochem. J. 364 (2002) 329–341.
[23] E.A. Olmsted-Davis, Z. Gugala, F.H. Gannon, P. Yotnda, R.E. McAlhany, R.W. Lindsey, A.R. Davis, Use of a chimeric adenovirus vector enhances BMP2 production and bone formation, Hum. Gene Ther. 13 (2002) 1337–1347.
[24] S. Knaan-Shanzer, M.J. van de Watering, I. van der Velde, M.A. Goncalves, D. Valerio, A.A. de Vries, Endowing human adenovirus serotype 5 vectors with fiber domains of species B greatly enhances gene transfer into human mesenchymal stem cells, Stem cells 23 (2005) 1598–1607.
[25] H. Tsuda, T. Wada, T. Yamashita, H. Hamada, Enhanced osteoinduction by mesenchymal stem cells transfected with a fiber-mutant adenoviral BMP2 gene, J. Gene Med. 7 (2005) 1322–1334.
[26] Z. Zhao, M. Zhao, G. Xiao, R.T. Franceschi, Gene transfer of the Runx2 transcription factor enhances osteogenic activity of bone marrow stromal cells in vitro and in vivo, Mol. Ther. 12 (2005) 247–253.
[27] X. Zhang, M. Yang, L. Lin, P. Chen, K.T. Ma, C.Y. Zhou, Y.F. Ao, Runx2 overexpression enhances osteoblastic differentiation and mineralization in adipose-derived stem cells in vitro and in vivo, Calcif. Tissue Int. 79 (2006) 169–178.
[28] Y. Fukuchi, H. Nakajima, D. Sugiyama, I. Hirose, T. Kitamura, K. Tsuji, Human placenta-derived cells have mesenchymal stem/progenitor cell potential, Stem Cells 22 (2004) 649–658.
[29] J.M. Gimble, A.J. Katz, B.A. Bunnell, Adipose-derived stem cells for regenerative medicine, Circ. Res. 100 (2007) 1249–1260.

THE JOURNAL OF BIOLOGICAL CHEMISTRY VOL. 285, NO. 20, pp. 15268–15, May 14, 2010

Pertussis Toxin Up-regulates Angiotensin Type 1 Receptors through Toll-like Receptor 4-mediated Rac Activation*[S]

Received for publication, October 15, 2009, and in revised form, March 8, 2010 Published, JBC Papers in Press, March 15, 2010, DOI 10.1074/jbc.M109.076232

Motohiro Nishida[‡], Reiko Suda[‡], Yuichi Nagamatsu[‡], Shihori Tanabe[§], Naoya Onohara[‡], Michio Nakaya[‡], Yasunori Kanaho[¶], Takahiro Shibata[‖], Koji Uchida[‖], Hideki Sumimoto[**], Yoji Sato[§], and Hitoshi Kurose[‡1]

From the [‡]Department of Pharmacology and Toxicology, Graduate School of Pharmaceutical Sciences, and the [**]Department of Biochemistry, Graduate School of Medical Sciences, Kyushu University, Fukuoka 812-8582, the [§]Division of Cellular and Gene Therapy Products, National Institute of Health Sciences, Setagaya, Tokyo 158-8501, the [¶]Department of Physiological Chemistry, Graduate School of Comprehensive Sciences and Institute of Basic Medical Sciences, University of Tsukuba, Tsukuba 305-8575, and the [‖]Graduate School of Bioagricultural Sciences, Nagoya University, Nagoya 464-8601, Japan

Pertussis toxin (PTX) is recognized as a specific tool that uncouples receptors from G_i and G_o through ADP-ribosylation. During the study analyzing the effects of PTX on Ang II type 1 receptor (AT1R) function in cardiac fibroblasts, we found that PTX increases the number of AT1Rs and enhances AT1R-mediated response. Microarray analysis revealed that PTX increases the induction of interleukin (IL)-1β among cytokines. Inhibition of IL-1β suppressed the enhancement of AT1R-mediated response by PTX. PTX increased the expression of IL-1β and AT1R through NF-κB, and a small GTP-binding protein, Rac, mediated PTX-induced NF-κB activation through NADPH oxidase-dependent production of reactive oxygen species. PTX induced biphasic increases in Rac activity, and the Rac activation in a late but not an early phase was suppressed by IL-1β siRNA, suggesting that IL-1β-induced Rac activation contributes to the amplification of Rac-dependent signaling induced by PTX. Furthermore, inhibition of TLR4 (Toll-like receptor 4) abolished PTX-induced Rac activation and enhancement of AT1R function. However, ADP-ribosylation of G_i/G_o by PTX was not affected by inhibition of TLR4. Thus, PTX binds to two receptors; one is TLR4, which activates Rac, and another is the binding site that is required for ADP-ribosylation of G_i/G_o.

PTX,[2] a major virulence factor of Gram-negative bacillus *Bordetella pertussis*, which causes whooping cough, is well established as a pharmacological tool for a specific inhibitor of G_i signaling. PTX is composed of A-protomer and B-oligomer, and A-protomer exerts ADP-ribosyltransferase activity on the α subunit of heterotrimeric G_i proteins ($G\alpha_i$), leading to inhibition of receptor-G protein coupling (1, 2), whereas B-oligomer of PTX recognizes and binds carbohydrate-containing receptors that deliver A-protomer into the cytosol (3). However, several reports have demonstrated that PTX has additional effects, such as enhancement of immune responses (4–6), increase in adenosine A_1 receptor density (7), and activation of tyrosine kinase, mitogen-activated protein kinase, and NF-κB (8–10). These effects of PTX are reported to be independent of G_i modification.

Angiotensin (Ang) II plays an important role in the regulation of hypertrophy and/or hyperplasia of cardiovascular cells (11–13). In cardiac fibroblasts, Ang II has been demonstrated to stimulate the processes related to extracellular matrix remodeling (14). The biological function of Ang II is mediated by Ang II receptors located on the plasma membrane. Two isoforms (type 1 (AT1) and type 2 (AT2)) of Ang II receptor have been identified, but most of the cardiovascular effects of Ang II are attributed to AT1R (15). AT1R belongs to the G_q-coupled receptor family. Stimulation of AT1R activates phospholipase C and increases $[Ca^{2+}]_i$ through the production of inositol 1,4,5-trisphosphate, leading to the modulation of fibroblast activities, such as cell proliferation and extracellular matrix protein synthesis (16).

An increase in AT1R density is one of the features to enhance fibrogenic responses of the heart. For example, an increase in AT1R density has been reported in the heart after myocardial infarction (17, 18) and in hearts from biopsies from patients with spontaneous intracerebral hemorrhage (19). Several cytokines, such as tumor necrosis factor (TNF)-α and interleukin (IL)-1β, have been reported to up-regulate AT1R (17, 20). However, the molecular mechanism responsible for the increase in AT1R density is still unknown.

Many studies suggest that low concentration of ROS acts as a second messenger in the cardiovascular system (21, 22). Stimulation of IL-1β and TNF-α induces ROS production through

* This work was supported by grants from the Ministry of Education, Culture, Sports, Science, and Technology of Japan (to M. Nishida, M. Nakaya, and H. K.); a grant-in-aid for scientific research on Innovative Areas (to M. Nishida); a grant-in-aid for scientific research on Priority Areas (to H. K.); and grants from the Nakatomi Foundation, Sapporo Bioscience Foundation, and Naito Foundation (to M. Nishida).

[S] The on-line version of this article (available at http://www.jbc.org) contains supplemental Tables 1 and 2 and Figs. 1–4.

The data discussed in this study have been deposited in the NCBI Gene Expression Omnibus (GEO) (http://www.ncbi.nlm.nih.gov/geo) and are accessible through GEO Series accession number GSE5017.

[1] To whom correspondence should be addressed. Tel./Fax: 81-92-642-6884; E-mail: kurose@phar.kyushu-u.ac.jp.

[2] The abbreviations used are: PTX, pertussis toxin; Ang II, angiotensin II; AT1R, Ang II type 1 receptor; DN-Rac and DN-p47^{phox}, dominant negative Rac and p47^{phox}, respectively; DPI, diphenyleneiodonium; GFP, green fluorescent protein; ct, carboxyl terminal region; IκBαm, non-phosphorylated form of IκBα, which works as a dominant negative mutant; IL, interleukin; MOI, multiplicity of infection; NF-κB, nuclear factor κB; IκB, inhibitor of κB; PH, pleckstrin homology; PI, phosphatidylinositol; PI-3-P, PI 3-phosphate; PLC, phospholipase C; PX, *phox* homology; Ro-106-9920, 6-(phenylsulfinyl)tetrazolo[1,5-*b*]pyridazine; ROS, reactive oxygen species; TNF-α, tumor necrosis factor-α; WT, wild type; ELISA, enzyme-linked immunosorbent assay; siRNA, small interfering RNA.

NADPH oxidase activation (23). A small GTP-binding protein, Rac, regulates the activity of NADPH oxidase (24) and mediates IL-1β- or TNF-α-induced ROS production and NF-κB activation (25). We have previously reported that Rac mediates Ang II-stimulated ROS production through NADPH oxidase activation in cardiac myocytes and cardiac fibroblasts (26, 27). Overexpression of constitutively active Rac1 induces hypertrophic responses in isolated cardiomyocyte and dilated cardiomyopathy *in vivo* (28, 29). Although a high concentration of hydrogen peroxide (H_2O_2) is reported to decrease AT1R density (30), it is unknown whether production of low concentration of ROS via Rac-mediated NADPH oxidase activation participates in the receptor-stimulated increase in AT1R density of cardiac cells.

Toll-like receptors (TLRs) play a critical role in both innate and adaptive immunity (31). There are at least 10 TLRs identified so far in humans, which specifically recognize and bind to a variety of pathogenic factors, including lipopolysaccharide. The mouse heart expresses at least six receptors (TLR2, -3, -4, -5, -7, and -9), and the stimulation of these receptors induces activation of NF-κB. TLR2 and TLR4 have been extensively studied in the heart, and both receptors are in part responsible for cardiac dysfunction in certain pathological conditions (32). Recent studies have elucidated that PTX functions as a superior ligand for TLR4 (6, 10). Although stimulation of TLR4 results in production of proinflammatory cytokines, it has not been reported that PTX exerts some pharmacological action(s) through TLR4 in cardiovascular cells, and it is unknown whether PTX-induced ADP-ribosylation of G_i/G_o requires TLR4-mediated entry into cells.

During the study of the role of G_i proteins in AT1R-mediated fibrotic responses using rat neonatal cardiac fibroblasts, we found that PTX enhances Ang II-induced increase in $[Ca^{2+}]_i$. Because we previously reported that the treatment with PTX increases Rac activity in rat neonatal cardiac myocytes (26), we hypothesized that Rac is implicated in PTX-induced enhancement of Ang II signaling in cardiac fibroblasts. In this study, we demonstrate that PTX B-oligomer induces Rac activation through a pathway independent of ADP-ribosylation of G_i/G_o. PTX increases IL-1β induction through sequential activation of TLR4, Rac, NADPH oxidase, and NF-κB, which leads to AT1R up-regulation through amplification of Rac-dependent signaling in rat cardiac fibroblasts.

EXPERIMENTAL PROCEDURES

Materials, Recombinant Adenoviruses, and Culture of Cardiac Fibroblasts—PTX, simvastatin, and anti-$G\alpha_{q/11}$ antibody were purchased from Calbiochem. Ang II was from Peptide Institute. Mastparan-7, ATP, wortmannin, and diphenyleneiodonium (DPI) were purchased from Sigma. Ro-106-9920 was from Tocris. Rat IL-1β and PTX B-oligomer were from Wako. Rabbit anti-rat IL-1β antibody and the rat IL-1β ELISA kit were from Endogen. Anti-$G\alpha_{11}$, anti-$PLC\beta_3$, anti-IκBα, anti-p65, anti-RhoA, anti-rabbit IgG, and anti-mouse IgG antibodies were purchased from Santa Cruz Biotechnology, Inc. (Santa Cruz, CA). [^{125}I]Ang II, [^{32}P]NAD, and glutathione-Sepharose beads were from Amersham Biosciences. Anti-Rac1 and anti-Rap1 antibodies were from Transduction Laboratories. Anti-Ras antibody was from Upstate Biotechnology. Anti-phospho-Akt and anti-Akt antibodies were from Cell Signaling. Fura2/AM was from Dojindo. 2,7-dichlorofluorescein diacetate and Alexa Fluor 488 goat anti-rabbit antibody were from Molecular Probes. Collagenase and Fugene 6 were from Roche Applied Science. Dual luciferase reagents were from Promega. pNF-κB-Luc and pRL-SV40 were from Stratagene. The sequences coding the Rap1-binding domain of Ral-GDS, Rac-binding domain of p21-activated kinase, Rho-binding domain of rhotekin, or Ras-binding domain of Raf were cloned, sequenced, and ligated into pGEX-4T-1 to make glutathione *S*-transferase fusion protein constructs. Glutathione *S*-transferase fusion proteins were expressed at room temperature and purified using gluthathione-Sepharose as described (33). The cDNA encoding GRP1-PH was provided by Dr. Alexander Gray (University of Dundee, Scotland). Recombinant adenoviruses of GRK2 (G protein-coupled receptor kinase 2)-ct, RGS4 (regulator of G protein signaling 4), WT $G\alpha_i$, $G\alpha_i$-ct, IκBαm, GFP-fused WT Rac, GFP-fused constitutively active Rac (G12V), DN-Rac (T17N), DN-$p47^{phox}$, and p115-RGS were produced as described previously (26, 34). Stealth siRNAs oligonucleotides for rat IL-1β, TLR4, and Rac1 were from Invitrogen. Sequences of stealth siRNA used were described in supplemental Table 1. Cardiac fibroblasts were prepared from ventricles of 1–2-day-old Sprague-Dawley rats, as described previously (27).

Quantification of Intracellular Ca^{2+} and ROS Concentration—$[Ca^{2+}]^i$ was measured by the method described previously (35). Briefly, cells (5×10^4) were plated on a 3 × 10-mm microcoverglass (MATSUNAMI) and loaded with 1 μM fura-2/AM in the cultured medium at 37 °C for 30 min. Cells were washed with HEPES-buffered salt solution containing 107 mM NaCl, 6 mM KCl, 1.2 mM $MgSO_4$, 0.5 mM EGTA, 20 mM HEPES (pH 7.4), and 11.5 mM glucose. Measurement of intracellular ROS concentration was performed in 2 mM Ca^{2+}-containing HEPES-buffered salt solution with a fluorescent dye, 2,7-dichlorofluorescein diacetate, as described previously (27). Fluorescence images were recorded and analyzed with a video image analysis system (Aquacosmos, Hamamatsu Photonics). The peak changes ($\Delta F/F_0$) of dichlorofluorescein fluorescence intensity were identified as values obtained by subtracting the basal fluorescence intensity (F_0) from the maximal intensity during a 15-min PTX treatment.

Measurement of IL-1β mRNA and Protein Expression—Expression of IL-1β mRNA and protein was measured by real time reverse transcription-PCR and ELISA, as described previously (36). For the preparation of real time reverse transcription-PCR analysis, cells (3×10^5) plated on 6-well dishes were treated with PTX for 24 h and lysed with 400 μl of RLT buffer (Qiagen). For ELISA, cells (1×10^5) on 12-well dishes were treated with PTX (100 ng/ml) in 500 μl of medium, and cells were then collected together with medium. After cells were homogenized with a 26-gauge syringe, 100 μl of supernatants were used. Assays were performed according to the manufacturer's instructions.

Microarray Analysis—Cells (1×10^6) plated on 35-mm dishes were treated with PTX for 24 h and lysed with 400 μl of RLT buffer. Total RNA was extracted with the RNeasy minikit (Qiagen) and RNase-free DNase set (Qiagen). Total RNA was converted to biotin-labeled cRNA, which was hybridized to the

rat genome U34A GeneChip (Affymetrix) for 16–24 h at 45 °C. The hybridization signals on the microarray were scanned and computed at a target intensity of 500 by a GeneChip Scanner 3000 and GeneChip Operating Software (Affymetrix), respectively. The data analysis was performed as follows. At the first step, probe sets without expression in the fibroblasts, which were indicated as absent by absolute analysis in more than half of the replicates in both the control and PTX-treated groups, were eliminated from the data set. Then, if the difference in the mean signal intensity of a given probe set was equal to the cut-off (1.25-fold) or more between the control and PTX-treated groups and if its p value calculated by Student's t test was less than 0.05, that probe set was employed. At the last step, probe sets with an annotation "signal transduction" (GO:0007165) in the AmiGO data base (available on the World Wide Web) were extracted, using the NetAffx Gene Ontology Mining Tool (available on the World Wide Web).

Ang II Binding Assay—Measurement of Ang receptor binding was performed according to the previous report (15) with a slight modification. After various treatments for 24 h, cardiac fibroblasts were rinsed with 10 ml of ice-cold phosphate-buffered saline and mechanically detached in 1 ml of ice-cold lysis buffer containing 10 mM Tris, pH 7.4, 5 mM EDTA, 5 mM EGTA, 1 μg/ml benzamidine, 10 μg/ml soybean trypsin inhibitor (type II-S), and 5 μg/ml leupeptin. The cell lysate was centrifuged at 45,000 × g for 10 min at 4 °C. The pellet containing crude membrane fraction was resuspended in 1 ml of ice-cold lysis buffer with a Potter type homogenizer, frozen, and stored at −80 °C until use. After the concentration of membrane protein was determined, membrane protein (20 μg) was used for the binding studies. The membrane was incubated with 0.1 nM ^{125}I-Ang II in 75 mM Tris, pH 7.4, 12.5 mM $MgCl_2$, 2 mM EDTA, and increasing concentrations of unlabeled Ang II (0–14 nM) for 1 h at 25 °C. Nonspecific binding was determined in the presence of 1 μM unlabeled Ang II. The reaction mixture was filtered over Whatman GF/C filters. The filters were washed with ice-cold buffer containing 25 mM Tris, pH 7.4, and 1 mM $MgCl_2$. The bound ^{125}I-Ang II on the filters was measured with a γ-counter. The values of K_d and B_{max} were calculated by Prism software (GraphPad Software, San Diego, CA).

Measurement of NF-κB Activity—After adenovirus was infected at 100 MOI for 2 h in serum-free medium, fibroblasts (3×10^5 cells) in a 24-well plate were transiently co-transfected with 0.45 μg of pNF-κB-Luc and 0.05 μg of pRL-SV40 control plasmid, using Fugene 6 (27). Luciferase activity was measured 48 h after transfection with dual luciferase reagents.

Measurement of Small GTPase Activities—Activation of small G proteins was determined as described previously (26). Activated Rac, Rho, Ras, and Rap1 were pulled down with 5 μg of glutathione S-transferase-fused Rac-interacting domain of p21-activated kinase (PAK-CRIB), Rho-binding domain of rhotekin (34), Ras-binding domain of Raf-1 (37), and Rap1-binding domain of Ral-GDS (38), respectively. Pulled-down small G proteins were detected with anti-Rac1, anti-RhoA, anti-Ras and anti-Rap1 antibodies. For knockdown of Rac1, cells were transfected with a mixture of Rac1 siRNAs (50 nM each) for 72 h.

Confocal Visualization of GFP-fused Proteins and NF-κB p65 Subunit—Cells (1×10^5) plated on glass bottom 35-mm dishes were infected for 24 h with GFP, GFP-Rac, GFP-constitutively active Rac, GFP fusion protein with PX domain of $p40^{phox}$ ($p40^{phox}$-PX), and $p40^{phox}$-PX (R105K). After the treatment with PTX (100 ng/ml) for 24 h, cells were fixed by 10% formaldehyde neutral buffer solution. For localization of NF-κB, cells were stained with anti-p65 antibody. Fluorescence images were measured at an excitation wavelength of 488 nm with a laser-scanning confocal imaging system (Carl Zeiss LSM510).

In Vitro PTX-catalyzed ADP-ribosylation Assay—*In vitro* ADP-ribosylation of $G\alpha_i$ proteins by PTX was performed as described previously (39) with a slight modification. Briefly, cardiac fibroblasts pretreated with or without 100 ng/ml PTX for 24 h were harvested with ice-cold lysis buffer containing 50 mM Tris (pH 7.5), 5 mM EDTA, 5 mM EGTA, 10 μg/ml benzamidine, 5 μg/ml aprotinin, and 5 μg/ml leupeptin. After centrifugation at 15,000 rpm for 10 min at 4 °C, the pellet was resuspended in lysis buffer. PTX was preactivated by incubation in the solution containing 50 mM Tris (pH 7.5), 5 mM ATP, 20 mM dithiothreitol, and 1 mg/ml bovine serum albumin for 30 min at 30 °C. Then activated PTX was added to the assay mixture, including 100 μg of the membrane, and incubated for 60 min at 30 °C. The final concentrations of all reagents in the assay mixture were as follows: 50 mM Tris (pH 7.5), 50 μM GDP, 10 mM thymidine, 5 μM NAD, 0.5 μM [^{32}P]NAD, 20 μg/ml PTX, 0.2 mg/ml bovine serum albumin, 1 mM ATP, and 4 mM dithiothreitol. The reaction was stopped by the addition of an excessive amount of ice-cold 50 mM Tris (pH 7.5), and the samples were centrifuged at 15,000 rpm for 10 min at 4 °C. The pellet was solubilized in SDS sample buffer, boiled, and subjected to 12% SDS-PAGE. Radioactive bands were detected by filmless autoradiographic analysis (BAS2000 system, Fujifilm).

Statistical Analysis—The results are presented as mean ± S.E. from at least three independent experiments. The representative data of time course experiments were plotted from one of three similar experiments that were performed with more than 20 cells. The mean values were compared with control by one-way analysis followed by Dunnet's t test (for three or more groups) or Student's t test (for two groups).

RESULTS

PTX Enhances Ang II-induced Ca^{2+} Release through AT1R Up-regulation—During the study of AT1R function in cardiac fibroblasts, we found that treatment with PTX enhances transient increase in $[Ca^{2+}]_i$ induced by Ang II at low concentration in the absence of extracellular Ca^{2+} (Fig. 1*A*). The EC_{50} value of Ang II for the changes in $[Ca^{2+}]_i$ increases was 464 ± 44 pM in control cells, whereas the EC_{50} value was decreased to 91 ± 33 pM in PTX-pretreated cells (Fig. 1*B*). However, the ATP-induced Ca^{2+} release was not affected by PTX (Fig. 1*C*). These results suggest that PTX selectively enhances Ca^{2+} response induced by AT1R stimulation. We also found that treatment with PTX for 24 h resulted in a 2-fold increase in maximal ^{125}I-Ang II binding activity (B_{max}) in comparison with PTX-untreated membrane (Fig. 1*D*). PTX increased AT1R density in a time-dependent manner, and more than 18 h was required for a 2-fold increase in AT1R density (supplemental Fig. 1). The

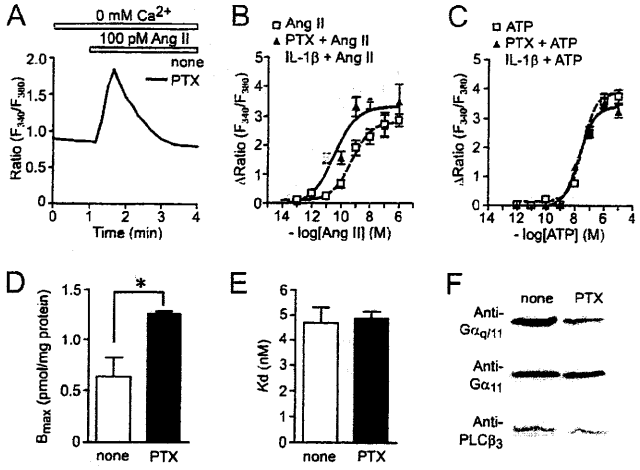

FIGURE 1. **PTX enhances Ca^{2+} responses by Ang II through AT1R up-regulation.** *A*, average time courses of Ca^{2-} response induced by Ang receptor stimulation with Ang II (100 pM) in control and PTX-treated cells. *B* and *C*, peak increases in $[Ca^{2+}]_i$ (*ΔRatio*) plotted against various concentrations of Ang II (*B*) and ATP (*C*) in control, PTX-treated, and IL-1β-treated cells. Cells were treated with PTX (100 ng/ml) or IL-1β (10 ng/ml) for 24 h before agonist stimulation. *D* and *E*, increases in AT1R density induced by PTX (100 ng/ml) for 24 h. The B_{max} (*D*) and K_d (*E*) values for Ang II binding were calculated with GraphPad Prism software. *F*, effects of PTX on expression of $G\alpha_{q/11}$ and $PLC\beta_3$. *, $p < 0.05$ *versus* PTX-untreated cells. *Error bars*, S.E.

PTX-induced increase in B_{max} was completely suppressed by CV11974 (1 μM, AT1R-selective blocker) but not by PD123319 (1 μM, AT2R-selective blocker) (data not shown). The K_d value was not affected by PTX (Fig. 1*E*), indicating that the PTX-induced enhancement of AT1R function is not explained by structural changes in AT1R. It has been reported that the increased expression of $G\alpha_{q/11}$ and $PLC\beta_3$ is involved in the enhancement of Ang II-induced Ca^{2+} responses in the ischemic heart (40, 41). However, PTX did not affect the expression levels of $G\alpha_q$, $G\alpha_{11}$, and $PLC\beta_3$ (Fig. 1*F*). These results suggest that the enhancement of Ang II-induced Ca^{2+} release in PTX-treated cells is due to AT1R up-regulation but not up-regulation of components of the $G\alpha_q$-$PLC\beta$ pathway.

Because commercially available PTX contaminates with other endotoxins, including lipopolysaccharide, it is possible that other endotoxins contribute to enhancement of AT1R function. Thus, we examined the effects of denatured PTX or PTX purchased from another manufacturer (Sigma) on AT1R functions. Pretreatment of PTX with heat significantly reduced the enhancement of Ang II-induced Ca^{2+} release induced by PTX (supplemental Fig. 1). In contrast, the Ang II-induced Ca^{2+} release was also enhanced by PTX purchased from Sigma as well as that induced by PTX from Calbiochem. These results suggest that PTX proteins *per se* induce AT1R up-regulation in cardiac fibroblasts.

IL-1β Production Induced by PTX Treatment—To examine whether PTX treatment induces production of a factor(s) that participates in up-regulation of AT1R, we performed microarray analysis of mRNAs from PTX-treated fibroblasts. For each gene, we calculated the average intensity in expression for both control and PTX-treated cells and plotted the ratio of these two induction values. Genes were chosen whose expression was at least 1.25-fold increased or decreased as compared with control cells. The probe sets of 405 genes showed significant changes by PTX treatment. Genes were then assigned to several groups according to their function, and we picked out 70 genes in the gene cluster that is termed "signal transduction" in the AmiGO data base (supplemental Table 2). PTX treatment selectively increased AT1R mRNA (Fig. 2*A*) but not other G protein-coupled receptors. Among genes increased by PTX treatment, IL-1α and IL-1β mRNAs showed a marked increase in expression (Fig. 2*A*). Real-time PCR confirmed the strong induction of IL-1β mRNA by PTX treatment (Fig. 2*B*). Although PTX is reported to increase IL-12 expression by inhibition of G_i signaling in T lymphocytes (42), PTX did not significantly increase mRNA expression of other cytokines (supplemental Table 1). Treatment with mastoparan-7 or the expression of WT $G\alpha_i$ or inhibitory polypeptides of G_i signaling ($G\alpha_i$-ct, a polypeptide that specifically inhibits receptor-G_i protein coupling (39); RGS4, a GTPase-activating protein that specifically binds the GTP-bound form of $G\alpha_i$ and $G\alpha_q$ (43); and GRK2-ct, a $G\beta\gamma$ ($\beta\gamma$ subunit of heterotrimeric G protein)-sequestering polypeptide (44)) did not increase IL-1β mRNA expression (Fig. 2*B*). We also confirmed that the expression of $G\alpha_i$-ct did not enhance Ang II-induced Ca^{2+} release (data not shown), and the treatment with B-oligomer of PTX enhanced Ang II-induced Ca^{2+} release (Fig. 2*C*). Furthermore, ELISA revealed that the treatment with PTX actually increased the expression of IL-1β protein levels, whereas the expression of IL-1α protein was below the detection level in PTX-treated cardiac fibroblasts (Fig. 2*D*). These results suggest that PTX selectively induces IL-1β production, and G_i modification is not required for PTX-induced IL-1β production.

IL-1β Mediates PTX-induced Enhancement of Ang II-induced Ca^{2+} Response—Because it has been reported that IL-1β increases AT1R density in cardiac fibroblasts (17, 45), the cells were treated with IL-1β. Treatment with IL-1β (10 ng/ml) enhanced Ang II-induced Ca^{2+} release (EC_{50} = 31 ± 26 pM) but not ATP-induced Ca^{2+} release, in rat cardiac fibroblasts (Fig. 1, *B* and *C*). These effects of IL-1β are similar to the effects of PTX treatment, and the enhancement by IL-1β seems to be consistent with the findings that PTX treatment increased the induction of IL-1β mRNA and protein. Thus, we examined whether PTX-induced IL-1β production participates in the enhancement of AT1R function. The PTX-induced IL-1β production was suppressed by the treatment with IL-1β siRNAs (Fig. 2*E*). The enhancement of Ang II-induced Ca^{2+} release by IL-1β treatment was almost completely suppressed by anti-IL-1β neutral antibody (Fig. 2*F*), indicating that the antibody sufficiently inhibits IL-1β-mediated responses. The enhancement of Ang II-induced Ca^{2+} release by PTX was also suppressed by anti-IL-1β antibody and IL-1β siRNAs (Fig. 2*G*), indicating that PTX-induced IL-1β secretion mediates the enhancement of Ang II-induced Ca^{2+} release.

Involvement of NF-κB in PTX-induced IL-1β Expression—As the promoter regions of IL-1β and AT1R contain a putative NF-κB binding site (46–48), we next examined the involvement of NF-κB in PTX-induced IL-1β production. As shown in Fig. 3*A*, PTX-induced increase in IL-1β mRNA expression was suppressed by the treatment with Ro-106-9920, a selective inhibitor of IκB phosphorylation, and by the expression of a dominant negative IκB, IκBαm. Because Ro-106-9920 showed

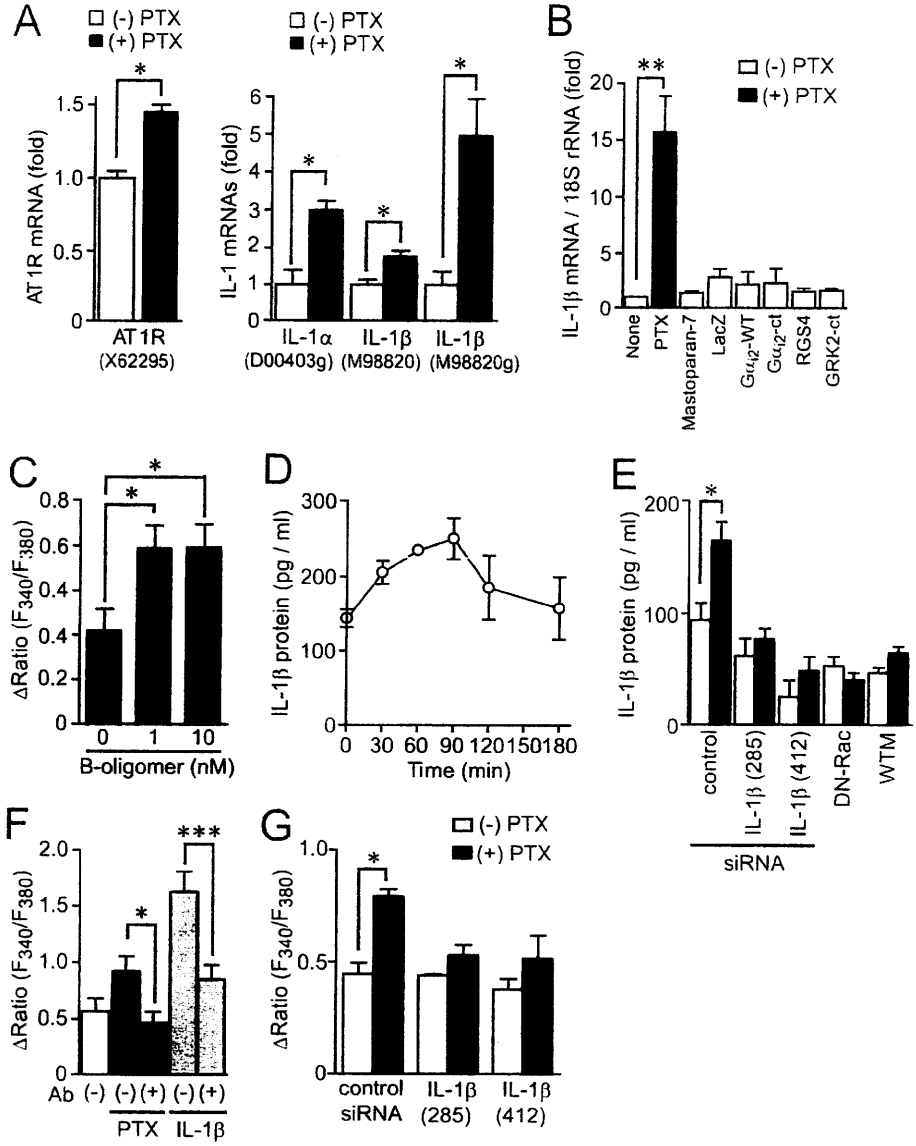

FIGURE 2. **Involvement of IL-1β production in PTX-induced enhancement of Ca^{2+} response by Ang II stimulation.** *A*, effects of PTX on the expression of AT1R, IL-1α, and IL-1β mRNAs. After cells were treated with PTX (100 ng/ml) for 24 h, total RNA was extracted. The expression of mRNAs was determined with microarray analysis. ID numbers of primer probe sets are shown in *parenthesis*. *B*, effects of respective reagents on IL-1β mRNA expression in cardiac fibroblasts. Cells were treated with PTX (100 ng/ml) for 24 h, treated with mastoparan-7 (10 μM) for 12 h, or infected with LacZ, WT $G\alpha_i$, $G\alpha_i$-ct, RGS4, and GRK2-ct at 300 MOI for 48 h. The -fold increases were calculated by the values of untreated cells (none) set as 1. *C*, effects of B-oligomer of PTX on Ang II-induced Ca^{2+} releases. Cells were treated with B-oligomer (1 or 10 nM) for 24 h before Ca^{2+} measurement. *D*, time course of PTX-induced expression of IL-1β protein. *E*, effects of IL-1β siRNAs, DN-Rac, and wortmannin (*WTM*) on PTX-induced IL-1β production. Two different siRNAs were used. *F* and *G*, effects of IL-1β neutral antibody (*F*) or IL-1β siRNAs (*G*) on Ang II-induced Ca^{2+} responses in control, PTX-treated, or IL-1β-treated cells. Cells were treated with PTX (100 ng/ml) or IL-1β (1 ng/ml) for 24 h before Ang II (100 pM) stimulation with or without anti-IL-1β antibody (500 μg/ml). Cells were transfected with IL-1β siRNAs (100 nM) 48 h before PTX treatment. *, $p < 0.05$; **, $p < 0.01$; ***, $p < 0.001$ *versus* PTX-untreated, B-oligomer-untreated, control siRNA-treated, PTX-treated, or IL-1β-treated cells. *Error bars*, S.E.

cytotoxic effects at higher concentration, we could not increase the concentration to observe complete inhibition of the IL-1β induction. The enhancement of AT1R function by PTX was suppressed by Ro-106-9920 and IκBαm (Fig. 3*B*), and the PTX-induced increase in AT1R density was suppressed by IκBαm (Fig. 3, *C* and *D*). Because an inhibition of NADPH oxidase activity suppresses NF-κB activation and IL-1β production induced by $G\alpha_{13}$ activation (36), we next examined the involvement of NADPH oxidase. Treatment with PTX increased NF-κB-dependent luciferase activity (Fig. 3, *E* and *F*). This NF-κB activation was suppressed by the treatment with DPI or by the expression of dominant negative (DN)-Rac and DN-$p47^{phox}$, both of which are essential for NADPH oxidase activation (24), but not by p115-RGS, a $G\alpha_{13}$-inhibitory polypeptide (26). These results suggest that PTX induces NF-κB activation through Rac-NADPH oxidase pathway and that NF-κB mediates PTX-induced IL-1β production and AT1R up-regulation.

Rac Mediates PTX-induced IL-1β Production and AT1R Up-regulation—We have previously reported in rat neonatal cardiomyocytes that PTX increases basal Rac activity (26). Because the PTX-induced NF-κB activation and IL-1β production was suppressed by DN-Rac (Figs. 2 and 3), we next examined whether PTX increases Rac activity in cardiac fibroblasts. Rac was activated from 10 min after PTX treatment and still activated at 24 h after the treatment (Fig. 4*A*). We also found that PTX did not affect the activities of other small G proteins, Ras, Rap1, and RhoA (supplemental Fig. 2). It has been reported that phosphatidylinositol (PI) 3-kinase participates in PTX B-oligomer-induced antiapoptotic action against HIV-Tat infection in NK cells (49). We confirmed that PTX B-oligomer increased Rac activity in cardiac fibroblasts (supplemental Fig. 3). Pretreatment with wortmannin completely suppressed PTX-induced Rac activation (Fig. 4*B*). The activated Rac has been reported to translocate from cytosol to the plasma membrane through recognition of membrane phospholipids, such as PI 3-phosphate (PI-3-P), PI 4-phosphate, PI 5-phosphate, and PI 3,4,5-trisphosphate, through the carboxyl-terminal polybasic region of Rac (50–52). Confocal imaging revealed that PTX actually translocated GFP-fused WT Rac from cytosol to the plasma membrane, as observed with constitutively active Rac (Fig. 4*C*). Pretreatment with wortmannin inhibited PTX-induced membrane localization of Rac. To demonstrate the involvement of PI-3-P, $p40^{phox}$-

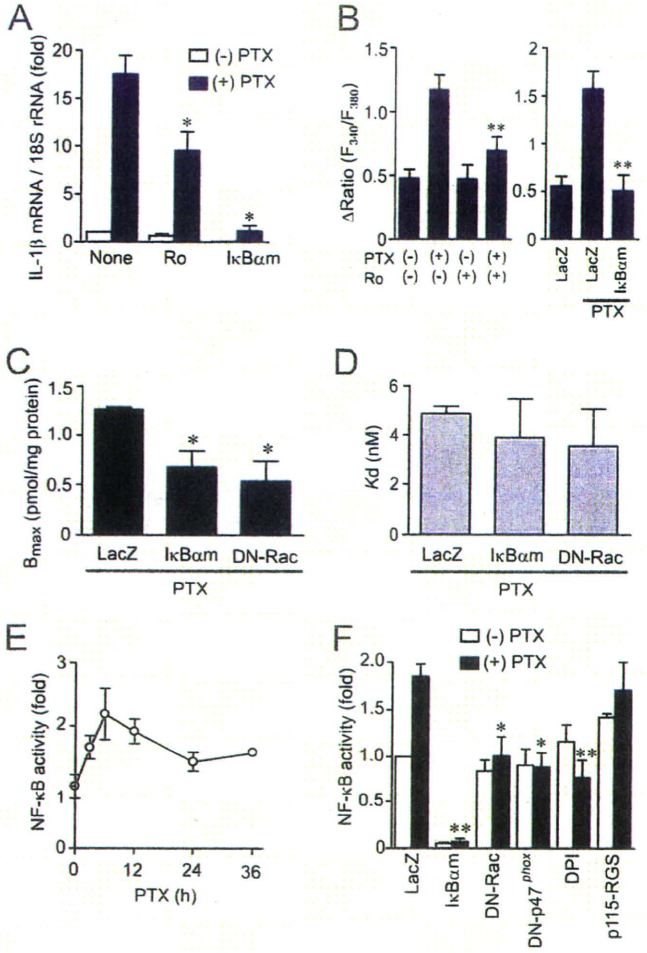

FIGURE 3. **Requirement of NF-κB for PTX-induced enhancement of Ca^{2+} response by Ang II stimulation.** *A*, effects of Ro106-9920 and IκBαm on PTX-induced IL-1β mRNA expression. Cells were pretreated for 20 min with Ro106-9920 (1 μM) or infected with IκBαm (100 MOI) for 48 h before the treatment of PTX (100 ng/ml) for 24 h. *B*, effects of NF-κB inhibitors on Ang II-induced Ca^{2+} responses in PTX-treated cells. *C* and *D*, effects of IkBαm and DN-Rac on PTX-induced increase in AT1R density. Cells were infected with adenoviruses expressing IkBαm or DN-Rac 24 h before PTX treatment. AT1R density was determined with receptor binding assay. *E*, time course of PTX-induced changes in NF-κB-dependent luciferase activity. *F*, effects of IκBαm, DN-Rac, DN-$p47^{phox}$, DPI, and p115-RGS on PTX-induced NF-κB activation. Cells were infected with LacZ, IκBαm, DN-Rac, DN-$p47^{phox}$, or p115-RGS at 100 MOI for 48 h or pretreated with DPI (5 μM) for 20 min before the addition of PTX (100 ng/ml) for 6 h. *, $p < 0.05$; **, $p < 0.01$ *versus* PTX-untreated or LacZ-expressing cells. *Error bars*, S.E.

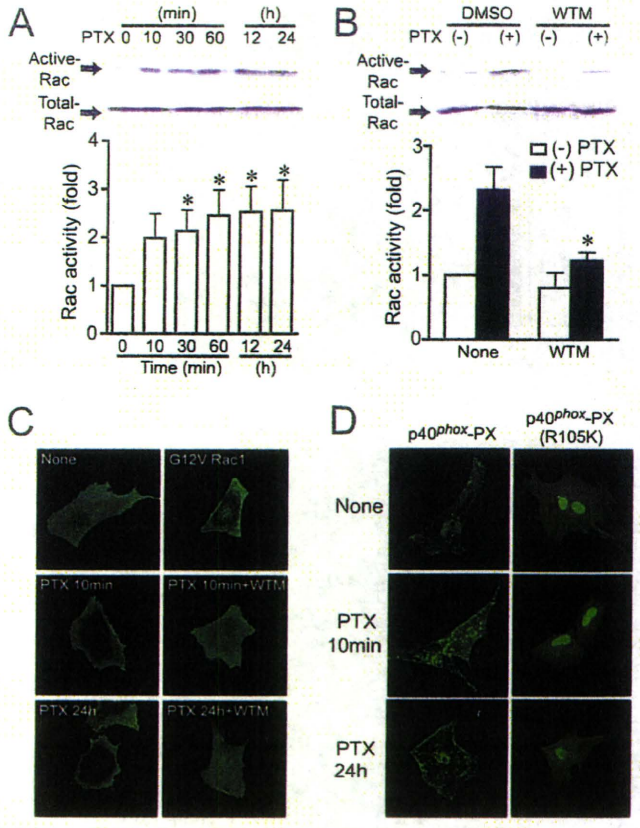

FIGURE 4. **PTX induces Rac activation.** *A*, time course of Rac activation induced by PTX (100 ng/ml). *B*, effects of wortmannin on PTX-induced Rac activation. Cells were pretreated with wortmannin (*WTM*; 100 nM) for 10 min before PTX stimulation. *C*, localization of GFP-fused wild type Rac and constitutively active Rac (*CA-Rac*) (G12V) with or without PTX stimulation. *D*, localization of GFP-fused PX domain of $p40^{phox}$ ($p40^{phox}$-PX), and PI-3-P interaction-deficient mutant ($p40^{phox}$-PX (R105K)) with or without PTX treatment. *, $p < 0.05$ *versus* PTX-untreated cells. *Error bars*, S.E.

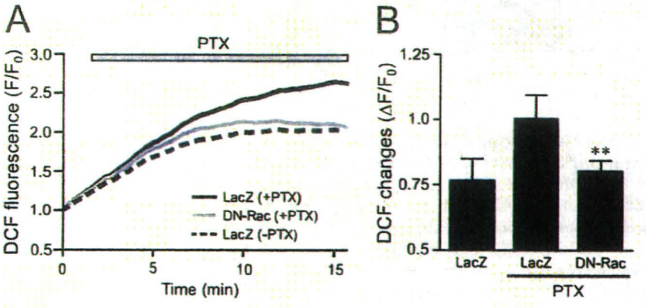

FIGURE 5. **Effects of DN-Rac on PTX-induced ROS production.** *A* and *B*, average changes (*A*) and peak increases (*B*) in PTX-induced F/F_0 of dichlorofluorescein from time course experiments. The increases in PTX-induced fluorescence of dichlorofluorescein were calculated by the value of maximal fluorescence intensity (*F*) during 20 min of stimulation and initial value of fluorescence, F_0. *, $p < 0.05$; **, $p < 0.01$ *versus* PTX-untreated or LacZ-expressing cells. *Error bars*, S.E.

PX, a specific marker for PI-3-P, was expressed (53). Under the basal condition, $p40^{phox}$-PX was predominantly localized in the PI-3-P-enriched early endosome and nucleus (Fig. 4*D*). Treatment with PTX for 10 min promoted the translocation of $p40^{phox}$-PX from early endosome to the plasma membrane. However, PTX did not affect the localization of $p40^{phox}$-PX (R105K), a mutant that cannot recognize PI-3-P. The localization of the PH domain of GRP1 (54), a marker for PI 3,4,5-trisphosphate, and that of the PH domain of PLCδ1, a marker for PI 4,5-bisphosphate, were not changed by PTX (data not shown). These results suggest that PTX-induced PI-3-P production through PI 3-kinase activation is required for translocation and activation of Rac.

Involvement of Rac in PTX-induced ROS Production—One of the targets for Rac is NADPH oxidase. Because the PTX-induced NF-κB activation was suppressed by DPI, DN-Rac, and DN-$p47^{phox}$ (Fig. 3*F*), Rac-mediated activation of NADPH oxidase may participate in PTX-induced NF-κB activation. We found that PTX gradually increased dichlorofluorescein fluorescence intensity, indicating ROS production in cardiac fibroblasts (Fig. 5). The expression of DN-Rac completely sup-

pressed this ROS production, suggesting that PTX activates Rac and turns on a signaling cascade downstream of Rac.

Essential Role of Rac in PTX-induced AT1R Up-regulation—Because PTX-induced ROS production, NF-κB activation, and increase in AT1R density were inhibited by DN-Rac, Rac may play a central role in regulation of AT1R density. Inhibitors of 3-hydroxy-3-methylglutaryl-CoA reductase (statins) are known to suppress the activity of Rho family G proteins by inhibition of isoprenylation (55). It has been reported that simvastatin inhibits Rac activity in the H9c2 cell line and rat neonatal cardiomyocytes (56, 57). Simvastatin is also reported to reduce AT1R density in vascular smooth muscle cells (58). Therefore, we examined whether simvastatin inhibits IL-1β-induced up-regulation of AT1R by inhibition of Rac. Treatment with simvastatin completely suppressed the IL-1β-induced Rac activation (supplemental Fig. 4). Consistent with this result, the IL-1β-induced up-regulation of AT1R was also suppressed by simvastatin and DN-Rac. The Ang II-induced Ca^{2+} release was also enhanced in IL-1β-treated cells, and this enhancement was completely suppressed by simvastatin. These results suggest that simvastatin suppresses IL-1β-induced up-regulation of AT1R by inhibition of Rac activity. To prove the requirement of Rac in AT1R up-regulation more directly, we used Rac1 siRNAs. Knockdown of Rac1 almost completely suppressed IL-1β-induced Rac activation (Fig. 6*A*), increase in AT1R density (Fig. 6*B*), and enhancement of AT1R-stimulated Ca^{2+} responses (supplemental Fig. 4). Thus, Rac1 may predominantly regulate AT1R up-regulation by agonist stimulation. Because IL-1β induces Rac activation and PTX-induced IL-1β production was completely suppressed by knockdown of Rac1 (Fig. 6*C*), we hypothesize that PTX-induced IL-1β production plays a role in amplification of Rac activation. Treatment with IL-1β siRNA suppressed the PTX-induced Rac activation at a late phase of activation (from 6 h after the treatment) but did not suppress Rac activation at an early phase of activation (Fig. 6, *D* and *E*). Furthermore, IL-1β siRNA also suppressed PTX-induced nuclear localization of NF-κB in a late phase but not an early phase (Fig. 6, *F* and *G*). These results suggest that PTX-induced IL-1β production participates in the sustained activation of Rac and NF-κB, which is essential for AT1R up-regulation.

PTX Stimulates TLR4, Leading to Rac Activation—We next examined which receptor(s) functions as a target of PTX in cardiac fibroblasts. Because TLR4 is reported to work as a putative candidate receptor of B-oligomer (10), we examined whether stimulation of TLR4 is required for PTX-induced AT1R up-regulation in cardiac fibroblasts. Treatment with TLR4 siRNAs (si-88, si-1002, and si-1621) significantly decreased TLR4 mRNA levels but did not decrease AT1R mRNA levels (Fig. 7*A*). The PTX-induced enhancement of Ang II-induced Ca^{2+} release and increase in Rac activity were completely abolished by TLR4 siRNA treatment (Fig. 7, *B* and *C*). In contrast, PTX-induced ADP-ribosylation of $G\alpha_i$ proteins was not suppressed but preferably enhanced by TLR4 knockdown (Fig. 7*D*). These results suggest that TLR4 mediates PTX-induced Rac activation and AT1R up-regulation, but TLR4 does not mediate PTX-induced ADP-ribosylation of $G\alpha_i$ proteins.

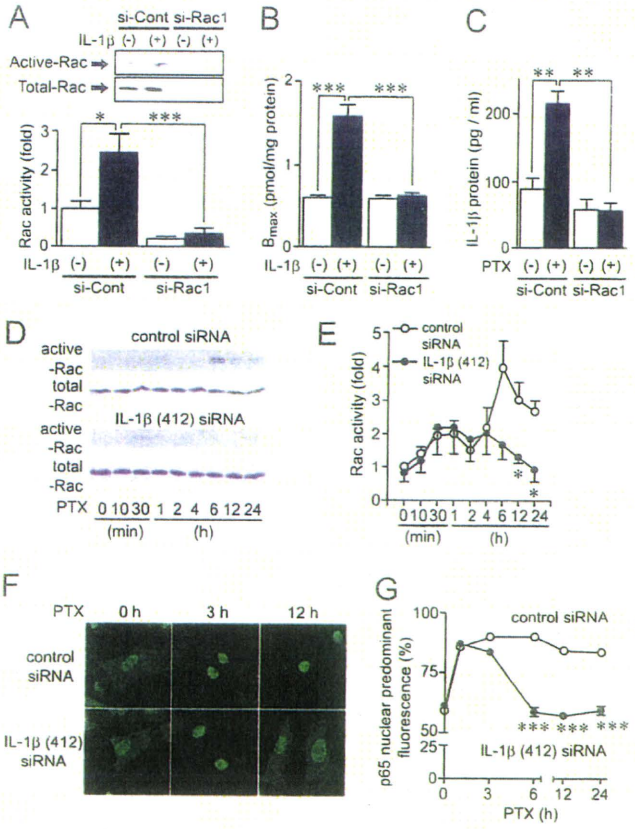

FIGURE 6. **Amplification of Rac-mediated signaling by PTX-induced IL-1β production.** *A*, cells were transfected with siRNAs for Rac1 (*si-Rac1*) or their randomized controls (*si-Cont*) for 72 h before 5-min stimulation with IL-1β (10 ng/ml). *B*, effects of si-Rac1 on the maximal increases in AT1R density by IL-1β stimulation. Cells were treated with IL-1β for 24 h before membrane preparation. *C*, effects of si-Rac1 on PTX-induced production of IL-1β proteins. Cells were treated with PTX (100 ng/ml) for 90 min. *D* and *E*, effects of IL-1β siRNA on PTX-induced Rac activation. Cells were transfected with IL-1β (412) siRNA (100 nM) for 48 h before treatment with PTX (100 ng/ml). *F* and *G*, effects of IL-1β (412) siRNA on PTX-induced nuclear localization of the NF-κB p65 subunit. More than 100 cells were scanned and quantified the subcellular localization of p65 using Photoshop (13, 27). *, $p < 0.05$; ***, $p < 0.001$ *versus* IL-1β-treated or control siRNA-treated cells. *Error bars*, S.E.

DISCUSSION

In this study, we demonstrated a novel action of PTX that enhances AT1R-stimulated Ca^{2+} response through AT1R up-regulation independently of ADP-ribosylation in rat cardiac fibroblasts. Using PTX as a powerful tool for analyzing the mechanism of AT1R up-regulation, we demonstrated that stimulation of TLR4 by PTX B-oligomer enhances AT1R function. Previous reports have suggested that Syk (spleen tyrosine kinase) and PI 3-kinase participate in TLR4-mediated responses (49, 59). We found that PTX-induced Rac activation was completely suppressed by inhibition of Syk (supplemental Fig. 3) and PI 3-kinase (Fig. 5), suggesting that Syk and PI 3-kinase mediate PTX-induced Rac activation. We also found that Rac-mediated NF-κB activation through ROS production plays a central role in the regulation of AT1R density. The PTX-induced NF-κB activation was suppressed by DPI and the dominant negative mutants of Rac and $p47^{phox}$ (Fig. 3). Because DPI is an inhibitor of NADPH oxidase and Rac and $p47^{phox}$ are essential compo-